© 2020. Published by The Company of Biologists Ltd | Journal of Cell Science (2020) 133, jcs244830. doi:10.1242/jcs.244830

RESEARCH ARTICLE

Phosphorylation and dephosphorylation of Ser852 and Ser889 control the clustering, localization and function of PAR3

Kazunari Yamashita[1,2], Keiko Mizuno[1], Kana Furukawa[1,3], Hiroko Hirose[1], Natsuki Sakurai[1], Maki Masuda-Hirata[1], Yoshiko Amano[1], Tomonori Hirose[1], Atsushi Suzuki[1,4] and Shigeo Ohno[1,*]

ABSTRACT

Cell polarity is essential for various asymmetric cellular events, and the partitioning defective (PAR) protein PAR3 (encoded by *PARD3* in mammals) plays a unique role as a cellular landmark to establish polarity. In epithelial cells, PAR3 localizes at the subapical border, such as the tight junction in vertebrates, and functions as an apical determinant. Although we know a great deal about the regulators of PAR3 localization, how PAR3 is concentrated and localized to a specific membrane domain remains an important question to be clarified. In this study, we demonstrate that ASPP2 (also known as TP53BP2), which controls PAR3 localization, links PAR3 and protein phosphatase 1 (PP1). The ASPP2–PP1 complex dephosphorylates a novel phosphorylation site, Ser852, of PAR3. Furthermore, Ser852- or Ser889-unphosphorylatable PAR3 mutants form protein clusters, and ectopically localize to the lateral membrane. Concomitance of clustering and ectopic localization suggests that PAR3 localization is a consequence of local clustering. We also demonstrate that unphosphorylatable forms of PAR3 exhibited a low molecular turnover and failed to coordinate rapid reconstruction of the tight junction, supporting that both the phosphorylated and dephosphorylated states are essential for the functional integrity of PAR3.

KEY WORDS: PAR3, PAR-3, ASPP2, aPKC, Epithelium, Polarity

INTRODUCTION

Cell polarity, one of the basic properties of cells, results in the asymmetric distribution of cell components and is governed by sets of evolutionarily conserved polarity-regulating factors, such as the PAR–atypical protein kinase C (aPKC) system. PAR proteins were first identified in the context of the asymmetric cell division of the *C. elegans* zygote (Kemphues et al., 1988). Mutations in these factors caused failures in the asymmetric cell division, and some of these proteins were found to asymmetrically localize to the anterior side or the posterior side (Etemad-Moghadam et al., 1995; Tabuse et al., 1998). The PAR–aPKC system functions in various asymmetric biological processes in animals, such as asymmetric cell division of stem cells, and establishment and maintenance of the asymmetric apical and basolateral membrane domain in epithelial cells (Izumi et al., 1998; Knoblich, 2001; Ohno, 2001; Suzuki and Ohno, 2006; Tepass et al., 2001). Although the molecules downstream of these factors are still under investigation, the basic concept for the mechanism of polarity establishment by the PAR–aPKC system has already been proposed; that is, mutual antagonism and positive-feedback enhancement. The apical determinant aPKC phosphorylates the basolateral regulators PAR1 [which has PAR1a (also known as MARK3), Par1b (MARK2), PAR1c (MARK1) and MARK4 isoforms in mammals] and Lgl (LLGL1 and LLGL2 in mammals) and excludes them from the apical domain (Betschinger et al., 2003; Suzuki et al., 2004; Yamanaka et al., 2003). Conversely, PAR1 phosphorylates the apical determinant PAR3 (encoded by *PARD3* in mammals) and excludes it from the lateral membrane domain (Benton and St Johnston, 2003b). In addition, Lgl inhibits the activity of aPKC (Yamanaka et al., 2003). The antagonistic relationship between apical determinants and basolateral determinants has been demonstrated using *Drosophila* genetics (Bilder et al., 2003; Tanentzapf and Tepass, 2003). The essentiality of the positive-feedback loop that enables self-recruitment of apical determinants has been demonstrated for aPKC and the Crumbs complex, another apical determinant protein complex, using both computer simulations and *in vivo* experiments (Fletcher et al., 2012).

In epithelial cells, the PAR3–aPKC–PAR6–Cdc42 complex (the PAR complex; note, in mammals, PAR6 is encoded by *PARD6A* and *PARD6B*) functions as an apical determinant. PAR3 localizes at the subapical membrane domain, the tight junction in mammalian epithelial cells and the adherens junction in *Drosophila*, whereas aPKC and PAR6 localize to both the tight junction and the apical membrane domain (Hirose et al., 2002; Morais-de-Sá et al., 2010). PAR3 localizes to primordial adherens junctions prior to other PAR complex components in mammalian epithelial cells (Suzuki et al., 2002), whereas Bazooka (the fly homolog of PAR3) is positioned through cytoskeletal cues, and acts upstream of adherens junctions to position and develop cadherin–catenin clusters in embryonic epithelia of *Drosophila* (Harris and Peifer, 2004, 2005). In both cases, PAR3 plays a unique role in the PAR complex by determining the initial formation of the PAR complex at the cell–cell contact region, a molecular landmark, that becomes the subapical region after polarity establishment (Román-Fernández and Bryant, 2016; Suzuki and Ohno, 2006). All of these observations, combined with other observations on the formation of the tight junction in epithelial cells, highlight the importance of PAR3 localization at a specific membrane domain during polarity establishment (Chen and Macara, 2005; Horikoshi et al., 2009).

PAR3 does not have a transmembrane domain, but it can interact with transmembrane proteins, such as JAM (Ebnet et al., 2001) and E-cadherin (Harris and Peifer, 2005), and can also interact with lipids, such as phosphatidic acid and phosphoinositides (Horikoshi et al., 2011; Krahn et al., 2010; Yu and Harris, 2012). These

[1]Department of Molecular Biology, Yokohama City University School of Medicine, Kanazawa-ku, Yokohama 236-0004, Japan. [2]Department of Molecular and Chemical Life Sciences, Graduate School of Life Sciences, Tohoku University, Aoba-ku, Sendai, Miyagi 980-8578, Japan. [3]Laboratory for Lung Development and Regeneration, RIKEN Center for Biosystems Dynamics Research, Kobe 650-0047, Japan. [4]Molecular Cellular Biology Laboratory, Yokohama City University Graduate School of Medical Life Science, Tsurumi-ku, Yokohama 230-0045, Japan.

*Author for correspondence (ohnos@med.yokohama-cu.ac.jp)

K.Y., 0000-0001-9222-5706; K.F., 0000-0001-9317-3856; H.H., 0000-0003-2428-0919; A.S., 0000-0002-3026-3026; S.O., 0000-0002-1294-5269

Handling Editor: Kathleen Green
Received 4 May 2020; Accepted 28 September 2020

Journal of Cell Science (2020) 133, jcs244830. doi:10.1242/jcs.244830

interactions can anchor PAR3 to the plasma membrane. The N-terminal oligomerization domain is essential for the localization of PAR3 (Benton and St Johnston, 2003a; Mizuno et al., 2003). The PAR3-binding protein ASPP2 (also known as TP53BP2) is also required for PAR3 localization to the tight junction region (Cong et al., 2010). Another study demonstrated that phosphorylations of Ser151 (corresponding to Ser144 of mammals) and Ser1085 (corresponding to Ser889 of mammals) in Bazooka/PAR3 by PAR1 result in the exclusion of Bazooka/PAR3 from the lateral membrane in *Drosophila* epithelial cells (Benton and St Johnston, 2003b; Hurd et al., 2003). However, how these mechanisms account for the regulation of PAR3 localization, and how these mechanisms relate to each other remain unclear.

In this study, we demonstrate that the ASPP2–PP1 complex dephosphorylates the novel phosphorylation site Ser852 of PAR3, and that dephosphorylation of Ser852 or Ser889 promotes cluster formation and accumulation of PAR3. This phosphorylation–dephosphorylation cycle could ensure the accumulation and turnover of PAR3, which is important for the rapid recruitment of PAR3 to the specific membrane domains where PAR3 acts as a landmark for other polarity regulators.

RESULTS

The interaction between PP1 and PAR3 is mediated by ASPP2, and is essential for proper PAR3 localization

As described above, ASPP2 is required for the localization of PAR3 to the tight junction (Cong et al., 2010). In addition to PAR3, ASPP2 can interact with a variety of proteins, including p53. This protein had also been identified as a subunit of protein phosphatase 1α (PP1α), suggesting that PAR3 can form a protein complex with ASPP2 and PP1 (Helps et al., 1995). Consistent with this, another study has demonstrated that PAR3 interacts with PP1α (Traweger et al., 2008). We hypothesized that ASPP2 could bridge the interaction between PAR3 and PP1α, and confirmed that PP1α was co-immunoprecipitated with PAR3 (Fig. 1A). Upon knocking down ASPP2, that amount co-immunoprecipitated PP1α was significantly decreased (Fig. 1A). To investigate the significance of the ASPP2–PP1α association on the regulation of PAR3, we used ASPP2 mutants lacking the interaction with PP1α. ASPP2 harbors an evolutionarily conserved RVKF stretch, which matches the PP1-binding consensus sequence, in its PP1-binding domain (Fig. 1B; Fig. S1A) (Egloff et al., 1997). We generated several mutants, including the previously reported ASPP2-REVD mutant (R921E and V922D) (Liu et al., 2011). This mutant was severely compromised in its interaction with PP1α (Fig. 1C). YAP (encoded by *YAP1*) and the LATS protein (LATS1 and LATS2), Hippo pathway factors, have been reported to interact with ASPP2. YAP binds to the proline-rich domain and the SH3 domain, and LATS proteins bind to the PP1α-binding domain of ASPP2 (Rotem et al., 2007; Vigneron et al., 2010). Although the ASPP2 mutant lacking the C-terminus (ASPP2-del3) failed to interact with YAP and LATS2, the REVD mutation did not affect the interaction with YAP and LATS2 (Fig. 1C,D). This suggests that the REVD mutation does not disrupt functions of ASPP2 other than binding to PP1α. We next expressed normal ASPP2 (ASPP2-WT) and ASPP2-REVD mutant in previously established ASPP2-knockdown MDCK cells (Cong et al., 2010). We observed that re-expression of ASPP2-WT rescued the cell–cell localization of PAR3, whereas the expression of the ASPP2-REVD did not (Fig. 1E,F; Fig. S1B). These results indicate that ASPP2 can act as an adaptor linking PP1 to PAR3, and suggest that this function is involved in the proper cell–cell localization of PAR3.

Ser852 of PAR3 is a novel phosphorylation site that acts as a 14-3-3-binding site

The significance of the ASPP2–PP1 interaction implies that dephosphorylation of PAR3 promotes the junctional localization of PAR3. In fact, several studies had already demonstrated that Ser144 and Ser889 are phosphorylated and serve as binding sites for 14-3-3 proteins, and that these phosphorylations regulate PAR3 localization and function (Fig. 2A) (Benton and St Johnston, 2003b; Hurd et al., 2003). Initially, we investigated whether phosphorylation of Ser144 or Ser889 was affected by the depletion of ASPP2. However, there were no significant effects on their phosphorylation levels (Fig. 3C,D). Therefore, we explored whether there were any unidentified 14-3-3-binding phosphorylation sites in PAR3. First, we performed far-western blotting using several His-T7-Xpress (HTX) tag-fused fragments of PAR3 and bacterially produced GST–14-3-3ζ as a probe. Among them, the 1–269 amino acid (aa) fragment exhibited weak affinity to 14-3-3ζ, whereas the 710–936 aa fragment showed a strong affinity (Fig. 2B). This result suggests that 14-3-3 proteins bind to phosphorylated Ser144 and Ser889, and that 14-3-3 proteins also recognizes other residues in the 710–936 aa fragment in addition to Ser889. Next, the transcriptional isoforms of PAR3 were subjected to far-western blotting. The short isoform of mouse PAR3 (sPAR3) that additionally lacks 827–856 aa (sPAR3-Δ827-856; sPAR3_ΔPB, RefSeq XP_006531595) and had been cloned in an earlier study (Hirose et al., 2002), was found to exhibit weaker affinity to 14-3-3ζ than did sPAR3, suggesting that important amino acid stretches are located in 827–856 aa (Fig. 2C). On this basis, we produced several serine residue point mutants and identified Ser852 as a novel 14-3-3-binding site in PAR3 (Fig. 2D). Ser852 appears to be conserved among vertebrates and chordates, whereas Ser144 and Ser889 are more widely conserved (Fig. 2E; Fig. S2A,B). We raised antibodies recognizing the respective phosphorylations at Ser852 and Ser889, and confirmed the phosphorylation of each serine residue (Fig. S2C). To evaluate the phosphorylation level of Ser144, we adopted the commercially available monoclonal antibody against the 14-3-3-binding consensus motif (K/RXXpSXP) because the sequence around Ser144 is the only stretch matching this consensus in PAR3 of mouse, rat and dog. In fact, we confirmed that this monoclonal antibody relatively specifically recognizes the phosphorylation of Ser144 (Fig. S2D,E). As it has been reported that Ser151 and Ser1085 of *Drosophila* Bazooka/PAR3 are phosphorylated by polarity-regulating kinase PAR1, we checked whether PAR1b (MARK2), one of the four mammalian orthologs of PAR1, phosphorylates Ser852 of PAR3. The amino acid sequence around Ser852 matches the consensus sequence of the PAR1 substrate reasonably well (Fig. S2F) (Nešić et al., 2010). In an *in vitro* kinase assay, it was observed that PAR1b phosphorylated the PAR3 842–876 aa fragment to the extent comparable to that of tau, an established substrate of PAR1b (Drewes et al., 1997), but it did not phosphorylate the S852A mutant fragment (Fig. 2F). Consistent with this, overexpression of PAR1b significantly upregulated the phosphorylation of both PAR3 Ser144 and Ser852 (Fig. 2G; Fig. S2G). We next evaluated whether endogenous PAR1 family kinases contribute to the phosphorylation of Ser852. Because siRNA appears to be unsuitable for inhibiting all of the four PAR1 homologs, we adopted the GFP-tagged MKI-peptide derived from *Helicobacter pylori* CagA, which inhibits PAR1 family kinases (Nešić et al., 2010; Saadat et al., 2007). We observed that MKI successfully inhibited the PAR1b overexpression-mediated phosphorylation of Ser144 and Ser852. However, it did not significantly inhibit the endogenous phosphorylation of Ser852 and other sites (Fig. 2H). Taken together, PAR1b can phosphorylate both Ser144 and Ser852 of PAR3. However, it is not only PAR1 family kinases but also other kinases that probably phosphorylate Ser144 and Ser852.

Journal of Cell Science (2020) 133, jcs244830. doi:10.1242/jcs.244830

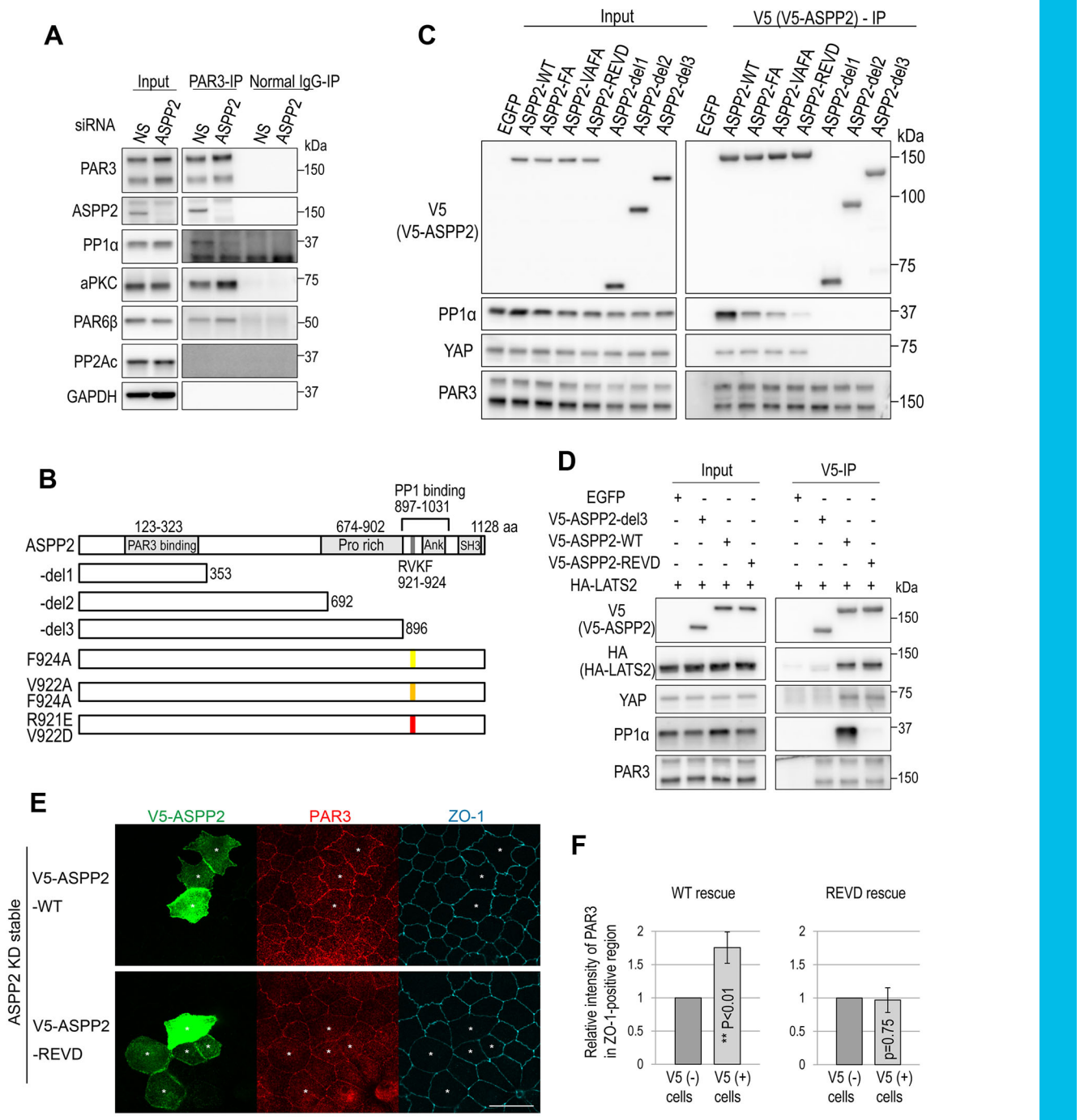

Fig. 1. ASPP2 is necessary for the interaction between PAR3 and PP1α, and the interaction between ASPP2 and PP1α is necessary for PAR3 localization. (A) MDCK cells were transfected with nonsilencing (NS) siRNA and siRNA against ASPP2. Then, immunoprecipitation (IP) was performed using anti-PAR3 or normal rabbit IgG. ASPP2 depletion decreased the co-immunoprecipitation of PP1α with PAR3 (long and short). (B) A schematic representation of the domain structure of ASPP2, its deletion mutants and point mutants as used in this study. (C) Interactions between ASPP2 mutants and PP1α or YAP were evaluated by immunoprecipitation. ASPP2 mutants were exogenously expressed in HEK293T cells. (D) Interactions between ASPP2 mutants and LATS2 or PP1α were tested by immunoprecipitation. For A, C and D the input is 5%. Images are representative of at least two, typically three, independent experiments. (E) V5–ASPP2-WT or V5–ASPP2-REVD mutants were expressed in the ASPP2-knockdown MDCK cells. Rescue of PAR3 localization was assessed. Asterisks indicate V5-ASPP2-expressing cells. (F) Quantification (mean±s.d.) of the fluorescence intensity of PAR3-staining in the tight junction region relative to control cells (set at 1) [~20 cells were measured in each sample, and four photos in two independent experiments were quantified (*n*=4)]. The precise method is described in Fig. S1B. Scale bar: 20 µm.

The ASPP2–PP1α complex dephosphorylates Ser852 of PAR3

We next evaluated whether Ser852 of PAR3 is a dephosphorylation target of the ASPP2–PP1α complex. We observed that depletion of ASPP2 upregulated the phosphorylation level of Ser852 (Fig. 3A,B). We also evaluated the phosphorylation levels of other sites, including Ser827, the target of aPKC (Nagai-Tamai et al., 2002). However, we could not detect any significant change in the phosphorylation levels other than that of Ser852. Owing to the poor specificity of the antibodies, PAR3 immunopurification was required for evaluation (Fig. 3C, lane 3 and 4; Fig. 3D). These

Journal of Cell Science

Journal of Cell Science (2020) 133, jcs244830. doi:10.1242/jcs.244830

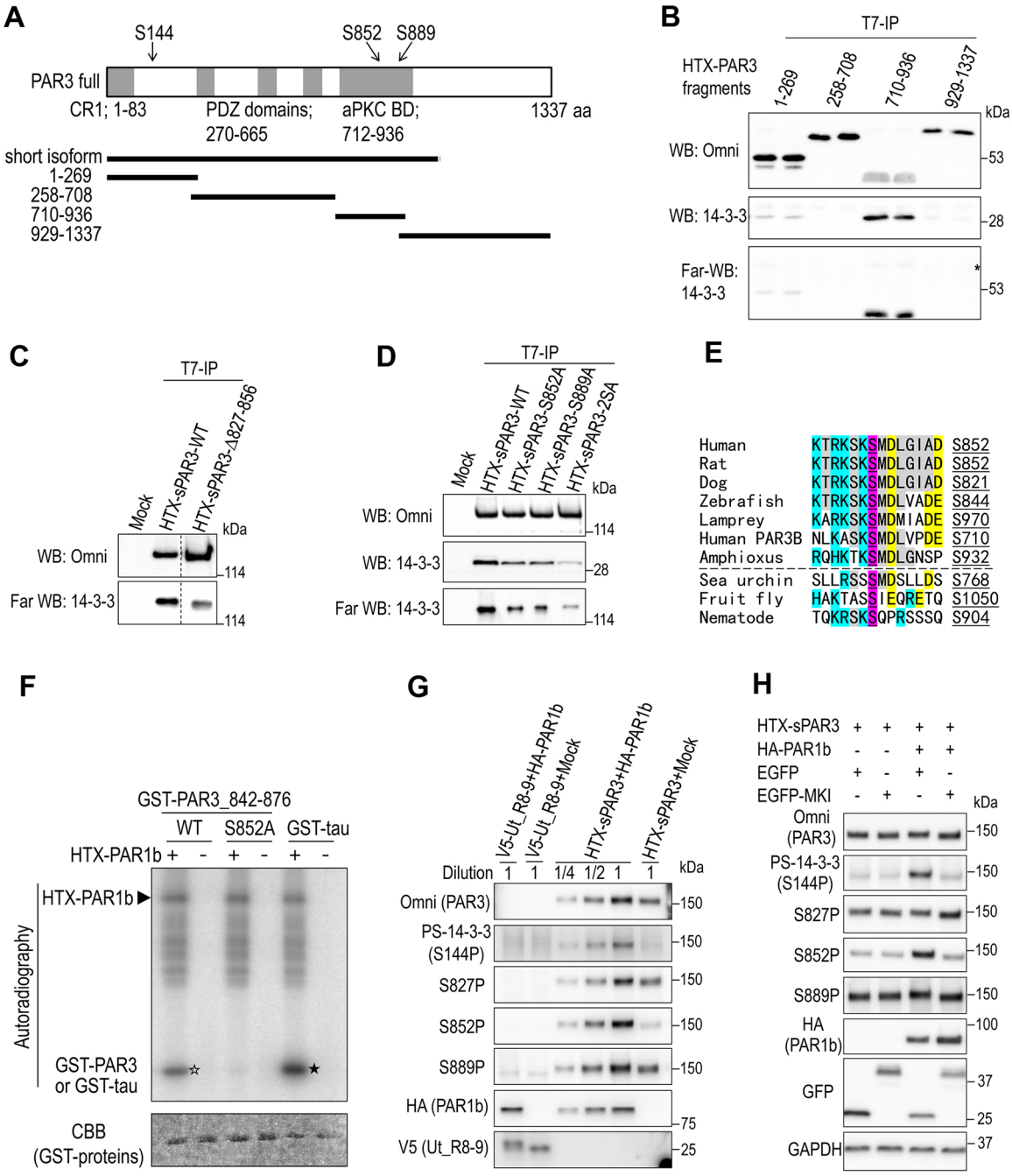

Fig. 2. Characterization of PAR3 phosphorylation – Ser852 is a novel phosphorylation site that is important for 14-3-3 binding. (A) A schematic representation of the domain structure of full-length PAR3, sPAR3 (the short isoform) and its fragments as used in this study. BD, binding domain. (B) Fragments of PAR3 were immunoprecipitated (IP) and analyzed by western blotting and far-western blotting using GST–14-3-3ζ as a probe. Omni-probe antibody recognizes a part of His-T7-Xpress tags (HTX) as an epitope. The asterisk indicates a non-specific signal. Duplicated experiments were performed and one representative experiment is shown. (C) PAR3 and PAR3-Δ827-856 deletion mutants were immunoprecipitated and analyzed by far-western blotting. (D) PAR3 and its point mutants were immunoprecipitated and analyzed by western blotting and far-western blotting. Both Ser852 and Ser889 were changed to alanine residues in the 2SA mutant. C and D are representative of two independent experiments. (E) Sequence alignment around Ser852 of PAR3. Magenta indicates Ser852, and blue, yellow and gray indicate basic, acidic and other common amino acids, respectively. Ser852 appears to be conserved among chordates, but conservation is not clear among metazoans. (F) *In vitro* kinase assay using immunoprecipitated PAR1b as a kinase source, and a GST-fused PAR3 fragment as a substrate. The open star indicates the phosphorylation of GST–PAR3_842-876, and phosphorylation was not observed in the S852A mutant. GST-tau peptide was used as a positive control (closed star). The arrowhead indicates the autophosphorylation of PAR1b. CBB, Coomassie Brilliant Blue staining. Representative of two independent experiments. (G) HEK293T cells were transfected with the indicated plasmids. Phosphorylation of PAR3 upon PAR1b overexpression was evaluated. Phosphorylation of Ser144 was monitored using the 14-3-3-binding consensus motif antibody [PS-14-3-3 (S144P)]. The lysate of PAR3- and PAR1b-overexpressing cells (lane 5) was diluted for the quantitative comparison (lanes 3 and 4). Mobility shift of V5-tagged spectrin repeats 8 and 9 of utrophin (Ut_R8-9) was used as a positive control for PAR1b-mediated phosphorylation (Yamashita et al., 2010). (H) HEK293T cells were transfected with each indicated plasmid. Promotion of PAR3 phosphorylation by PAR1b-overexpression and the inhibitory effect of MKI on PAR1b were evaluated. EGFP–MKI almost completely inhibited PAR1b overexpression-mediated phosphorylations (lanes 3 and 4), whereas it did not inhibit the endogenous phosphorylation of PAR3 (lanes 1 and 2). G and H are representative of two independent experiments.

Journal of Cell Science (2020) 133, jcs244830. doi:10.1242/jcs.244830

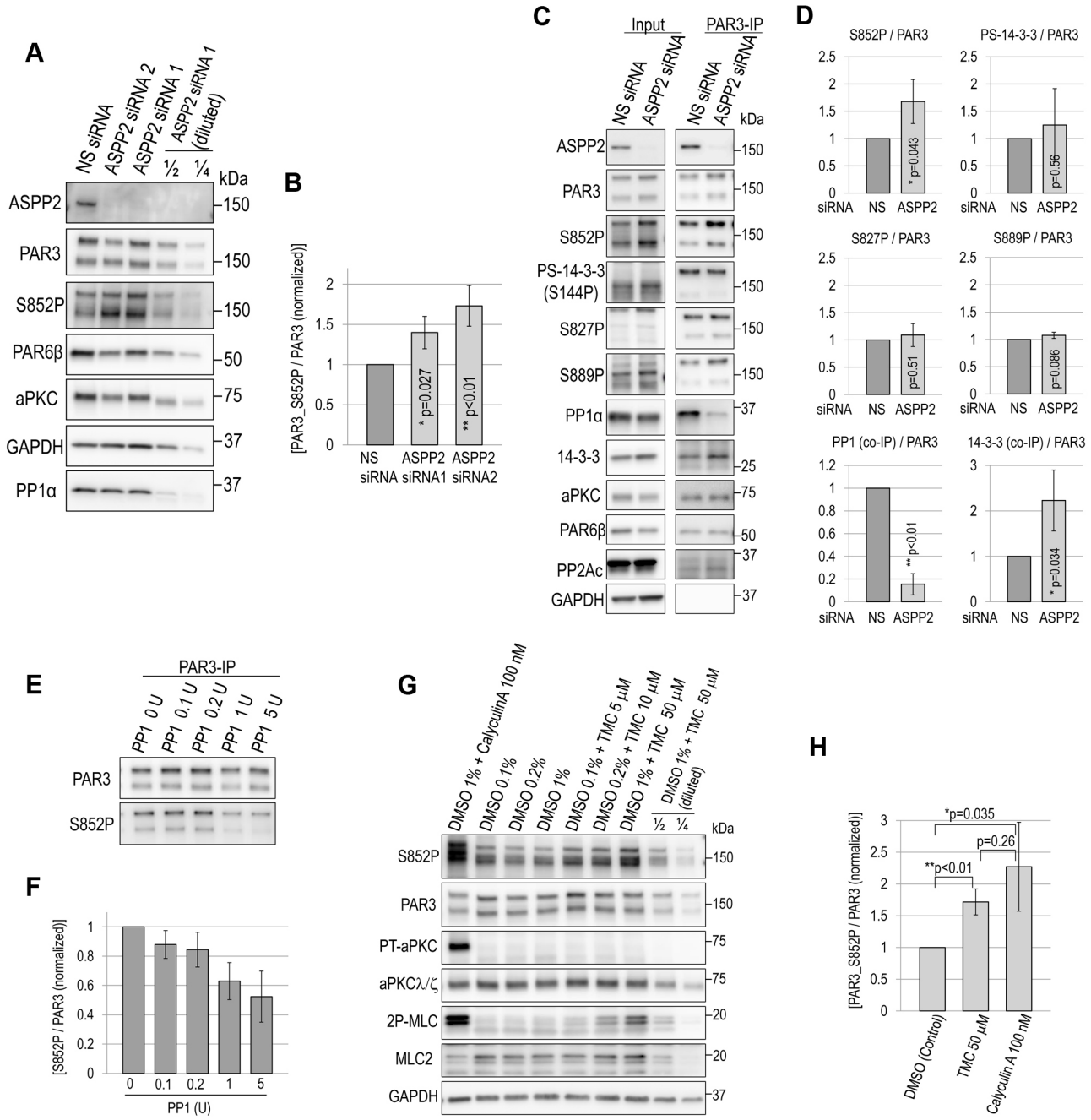

Fig. 3. ASPP2 and PP1α negatively regulate the phosphorylation level of Ser852 in PAR3. (A) MDCK cells were transfected with each indicated siRNA, and whole-cell lysates were analyzed by western blotting. A dilution series of the lysates from ASPP2 siRNA1-transfected cells was prepared for the quantification of Ser852 phosphorylation (S852P). (B) Quantification (mean±s.d.) of the phosphorylation levels of Ser852 from experiment shown in A (*n*=3). The signal intensity of S852P was normalized to the signal intensity of total PAR3. Student's *t*-test was used for statistical analysis; each siRNA transfected sample was compared with NS siRNA transfected control (set at 1). (C) PAR3 was immunoprecipitated (IP) from cells that were transfected with each siRNA. Then, the phosphorylation levels and the co-immunoprecipitation with interacting proteins were analyzed. To evaluate the phosphorylation levels of S144, S827 and S889, immunopurified PAR3 was analyzed. Phosphorylation of Ser144 was monitored using the 14-3-3-binding consensus motif antibody [PS-14-3-3 (S144P)]. The input is 5%. (D) Quantification (mean±s.d.) of the phosphorylation levels of PAR3 or co-immunoprecipitation in experiment C (*n*=3). (E) PAR3 was immunopurified from MDCK cells, and recombinant PP1α was treated. After incubation, the phosphorylation levels of Ser852 were assayed by western blotting. (F) Quantification (mean±s.d.) of Ser852 phosphorylation in experiment E (*n*=3). (G) MDCK cells were treated with the indicated concentrations of calyculin A and tautomycetin (TMC) for 1 h using DMSO as a vehicle. Treatment with both calyculin A and tautomycetin promoted the phosphorylation of PAR3 Ser852 and myosin regulatory light chain (2P-MLC), whereas only calyculin A promoted the phosphorylation of aPKCλ/ζ at Thr412/410. (H) Quantification (mean±s.d.) of Ser852 phosphorylation in experiment G (*n*=3). Each bracket indicates two groups analyzed by Student's *t*-test.

results suggest that the ASPP2–PP1α complex is involved in the dephosphorylation of Ser852. Next, we assessed the involvement of PP1. The phosphorylation level of Ser852 significantly decreased in a PP1α dose-dependent manner in an *in vitro* dephosphorylation assay (Fig. 3E,F). PP1α also efficiently dephosphorylated other sites, especially Ser144 and Ser827, suggesting that PP1α can dephosphorylate several sites (Fig. S3A,B). Taken together with the ASPP2-knockdown experiment, this suggests that PP1α is not the

Journal of Cell Science (2020) 133, jcs244830. doi:10.1242/jcs.244830

only factor that can mediate the dephosphorylation of Ser144 and Ser827. The significance of PP1 on Ser852 was also confirmed using the PP1-specific inhibitor tautomycetin (Choy et al., 2017; Mitsuhashi et al., 2001). Treatment with tautomycetin upregulated the phosphorylation of Ser852 of PAR3 and Thr18/Ser19 of the myosin light chain 2 (MYL2) without affecting Thr412/Thr410 of aPKCλ or aPKCζ and total phospho-threonine, whereas treatment with calyculin A, a broad Ser/Thr phosphatase inhibitor (Zhang et al., 2013a), upregulated all of the phosphorylations that we had tested, supporting the specificity of tautomycetin (Fig. 3G,H; Fig. S3C). This result would suggest that PP1 specifically functions in Ser852 dephosphorylation. However, we do not exclude the possibility of the involvement of other phosphatases, including PP2A, on Ser852 dephosphorylation, because calyculin A treatment was relatively more effective than tautomycetin treatment, although no significant difference was found between them (Fig. 3G,H). All of these data support the notion that ASPP2-associated PP1 dephosphorylates Ser852 of PAR3.

Dephosphorylated PAR3 can localize to the cell–cell junction irrespective of ASPP2 expression

Immunofluorescence experiments showed that both sPAR3-WT and the -S852A mutant localized to the tight junction region (Fig. 4A,B). Even in ASPP2-knockdown cells, sPAR3-S852A strongly localized to the tight junction region, although the localization of sPAR3-WT was disrupted (Fig. 4A,B). These results indicate the critical role of the ASPP2–PP1α complex in PAR3 localization and dephosphorylation of Ser852. The phosphorylation of Ser852 was remarkably inhibited by treatment with the nonspecific kinase inhibitor staurosporine (Fig. 4C), and staurosporine treatment also promoted the cell–cell junction localization of exogenously expressed sPAR3 (Fig. 4D). This result supports the critical importance of the phosphorylation of Ser852, and shows that dephosphorylation of Ser852 promotes the localization of PAR3 to cell–cell junctions.

PAR3-S852A and -S889A mutants tend to organize in ectopic protein clusters and fail to rescue the early step of tight junction formation

Next, we explored the physiological function of Ser852 phosphorylation. For this purpose, we established MDCK cell lines in which endogenous PAR3 was replaced by exogenous EGFP-fused PAR3 and its mutants (PAR3-rescued cells). S852A, S144A, S889A, the S852A/S889A double-mutant and the S144A/S852A/S889A triple-mutant were used to evaluate the function of each site. Their expression levels were ∼10-times greater than the endogenous level (Fig. S5A–C). Using these cell lines, we evaluated junction formation by performing a Ca^{2+} switch assay. In this assay, the cell–cell junction is disrupted by incubation in low Ca^{2+} concentration medium. Then, upon replacing the medium with normal Ca^{2+} concentration medium, the cell–cell junction is reorganized (Hirose et al., 2002).

Through this analysis, we discovered that S852A and S889A mutants were distributed as puncta in the cell–cell junction-disrupted cells (Fig. 5A,D). In several animal species, PAR3 has been observed as puncta, and this structure is thought to be organized by oligomerization-mediated clustering of PAR3 (Benton and St Johnston, 2003a; Feng et al., 2007; Harris, 2017; Inaba et al., 2015; Mizuno et al., 2003; Tabuse et al., 1998). On this basis, our result suggests that the dephosphorylation of Ser852 or Ser889 tends to cause clusters. Supporting this notion, PAR3 clusters were also observed in PAR3-WT–EGFP-expressing cells treated with staurosporine (Fig. S5D). These clusters merged with aPKC, PAR6β and ASPP2, but not with GP135 (also known as podocalyxin), suggesting that these puncta are not vacuolar apical compartments (VACs) and that these clusters contain the PAR–aPKC complex (Fig. S5D,E). Tight junction formation, which was indicated by ZO-1 (also known as TJP1) staining, was not as severely disrupted in all PAR3-rescued lines compared to that in the PAR3-knockdown cell line (Fig. 5E; Fig. S5G) (Chen and Macara, 2006; Horikoshi et al., 2009). Although all of these PAR3-rescued lines formed almost complete linear tight junctions at 2 h after the addition of a normal Ca^{2+} medium (Fig. S5F), the cell lines rescued with S852A, S889A and S852A/S889A mutants exhibited an obvious defect in tight junction formation at 30 min after the addition of the normal Ca^{2+} medium compared to that in PAR3-WT-rescued lines (Fig. 5C,E; Fig. S5G). These results indicate that phosphorylations that function to inhibit cluster formation are essential for the early step of tight junction formation. This could be because clustering prevents PAR3 recruitment owing to the clustering-mediated restriction of molecular diffusion, because an increased molecular size decreases the diffusion rate (Höfling and Franosch, 2013; Lippincott-Schwartz et al., 2001). In addition to this mechanism, it is possible that the interaction between PAR3 and cellular structures, such as microtubules and vesicles, could trap PAR3 clusters and prevent diffusion of dephosphorylated PAR3 (Chen et al., 2013; Jouette et al., 2019). Cell lines rescued by PAR3-S144A also exhibited a weaker defect in tight junction formation. This mutation may compromise the tight junction-inducing activity of PAR3, as discussed later.

Unphosphorylatable PAR3 mutants exhibited a low turnover at developing cell–cell junctions

Cluster formation could alter the kinetics of PAR3. Therefore, we evaluated the turnover rate of PAR3–EGFP at cell–cell junctions by fluorescence recovery after photobleaching (FRAP). We observed that fluorescence was recovered after the bleaching process uniformly throughout the cell–cell contact, suggesting that the newly supplied PAR3–EGFP was primarily derived from the cytoplasm, not from the adjacent plasma membrane (Fig. 6A,B; Fig. S6A). There were no significant differences in the mobile fraction and the half time of recovery for PAR3-S852A in confluent cultures (see also Discussion). The half time of recovery of PAR3-2SA (S852A/S889A) appeared to be prolonged in #6 clone (Fig. 6A,C,E) but was not reproduced in clone #3 (Fig. S6B). However, in developing cell–cell junctions, the half time of recovery of both S852A and 2SA (S852A/S889A) mutants was significantly longer than that of WT PAR3, although no significant difference was observed in the mobile fraction (Fig. 6B,D,F; Fig. S6C). These results support the notion that a low diffusion rate of clustered PAR3 prevents efficient recruitment of PAR3 to cell–cell junctions.

S852A, S889A and S852A/S889A mutants of PAR3 ectopically localize at the lateral membrane, and induce the ectopic localization of tight junction components

Ectopic localization of Ser151A and Ser1085A Bazooka/PAR3 mutant proteins to the lateral membrane domain has been observed in *Drosophila* (Benton and St Johnston, 2003b). In confluent cultures, we found that WT PAR3 and its mutants primarily localized around tight junctions. However, S852A, S889A, S852A/S889A and S144A/S852A/S889A mutants also partially localized to the lateral membrane domain (Fig. 7A). Moreover, in the cells expressing S852A, S889A and S852A/S889A mutants, tight junction components were ectopically localized to the lateral membrane

Journal of Cell Science (2020) 133, jcs244830. doi:10.1242/jcs.244830

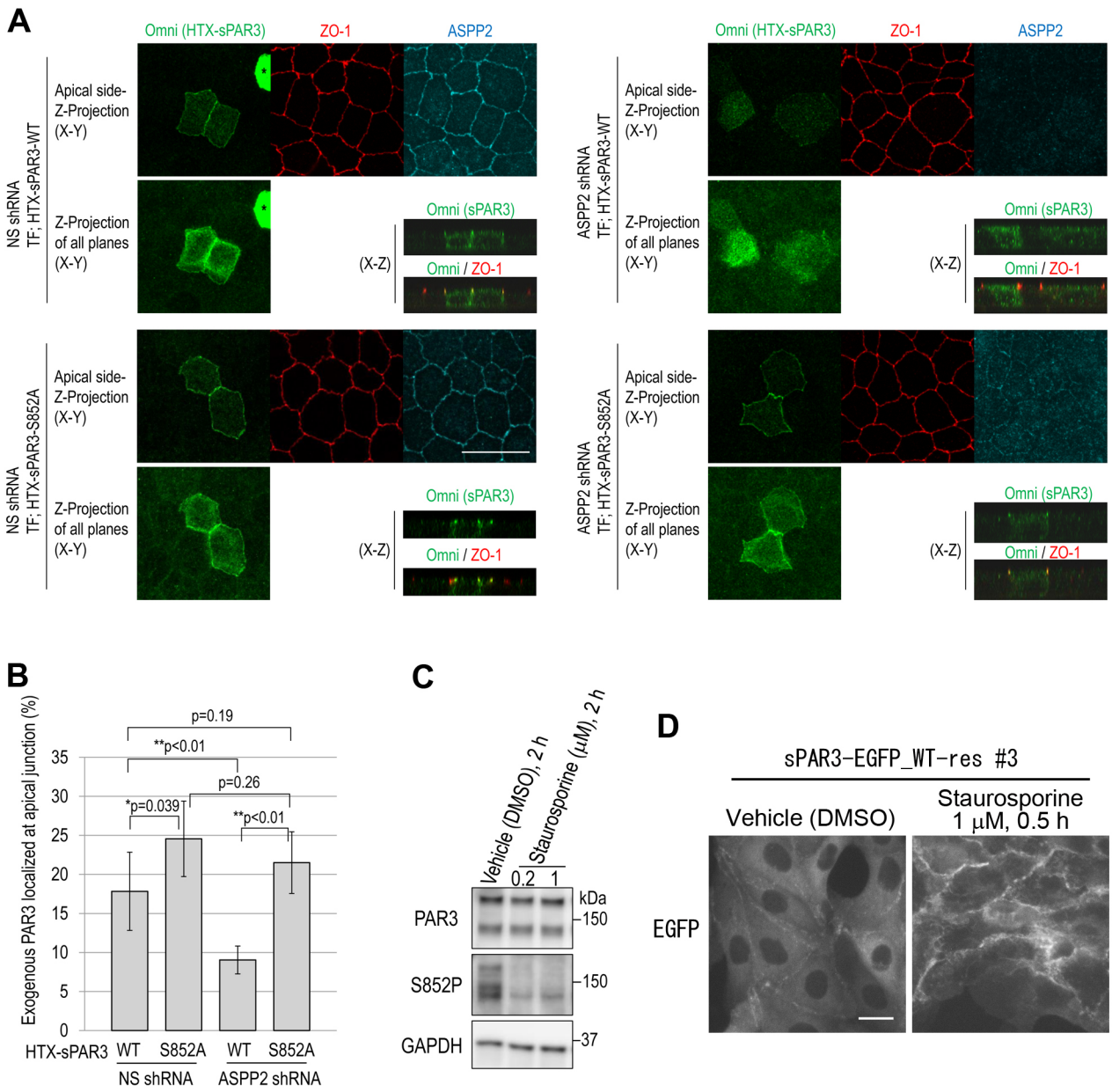

Fig. 4. PAR3-S852A strongly localized to the tight junction region irrespective of ASPP2 expression. (A) MDCK cells stably expressing nonsilencing shRNA and MDCK cells stably expressing ASPP2 shRNA were transfected with His-T7-Xpress-tagged sPAR3 wild-type or S852A mutant. Immunofluorescence staining was performed, and samples were observed by confocal microscopy. The percentage of tight junction region-localized PAR3 in total PAR3 was compared. To achieve this, we prepared the sum projection of *X*–*Y* sections where ZO-1-staining was positive (upper panels) and the sum projection of all *X*–*Y* sections (lower panels). Because most of overexpressed sPAR3 was localized in the cytoplasm (asterisks), we only quantified the cells expressing low level of sPAR3, by thresholding on the intensity. (B) Signal intensities of these images obtained as in A were quantified [mean±s.d.; ∼15 cells were measured in each sample, and six photos in two independent experiments were quantified (*n*=6)]. The precise method is described in Fig. S4. Each bracket indicates two groups analyzed by Student's *t*-test. (C) MDCK cells were treated with the indicated concentration of staurosporine for 2 h at 37°C. Then, the phosphorylation level of Ser852 (S852P) was evaluated by western blotting. (D) sPAR3–EGFP stably expressing MDCK cells were treated with 1 µM staurosporine for 30 min at 37°C, and localization of sPAR3–EGFP was analyzed. Scale bars: 20 µm.

domain (Fig. 7A,B; Fig. S7A). This suggests that extension of the tight junction region was induced by the ectopically localized PAR3 mutant proteins. When cultured for an additional 2 days, these cells organized unique intercellular structures, which contained ZO-1 and appeared as 'tubular invaginations' (Fig. S7B,C). These structures may have been formed by the fracturing of the extended tight junction, presumably because of the absence of adherens junctions, which mechanically link cell–cell contacts. This cell morphology is reminiscent of EpCAM-depleted epithelial cells (Salomon et al., 2017). Taken together, these results indicate that dysregulation of PAR3 localization leads to ectopic tight junction formation and morphological defects in the epithelial cell layer.

DISCUSSION

In this study, we demonstrated that Ser852 of PAR3, the novel 14-3-3-binding phosphorylation site, can be dephosphorylated by the ASPP2–PP1α protein complex and that dephosphorylation of Ser852 and Ser889 promoted the clustering of PAR3. Comparing with the

Journal of Cell Science (2020) 133, jcs244830. doi:10.1242/jcs.244830

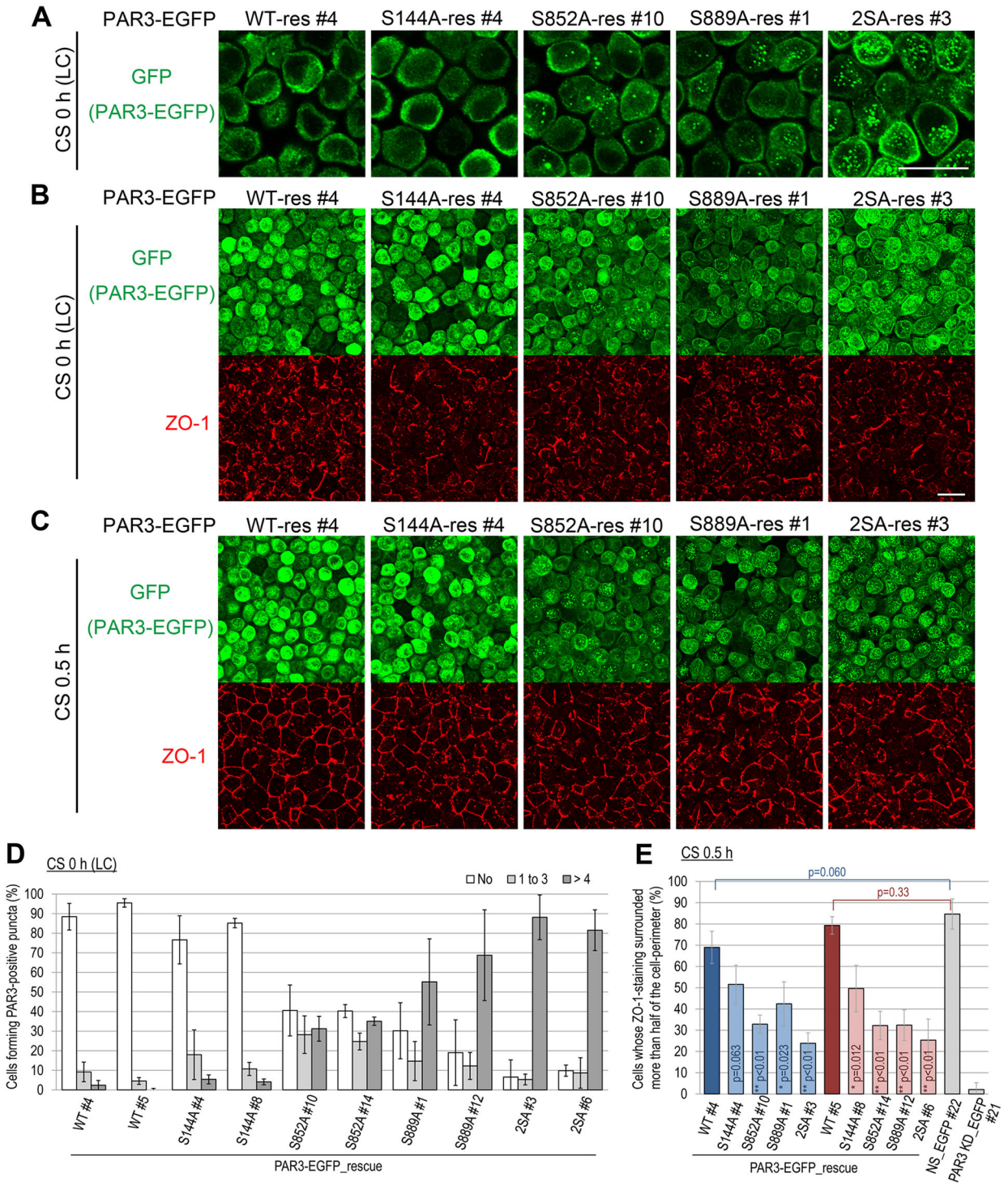

Fig. 5. PAR3-S852A and S889A mutants organized ectopic protein clusters and failed to rescue the rapid recovery of ZO-1-staining in a Ca^{2+} switch assay. (A) Wild-type PAR3 and its point mutants were fused with EGFP and stably expressed in the PAR3-knockdown MDCK cell line. These transformant MDCK cell lines were cultured in low-Ca^{2+} (LC) medium for 18 h. Then, immunofluorescence analysis was performed. One confocal section is displayed. (B) Maximum intensity projection (MIP) of confocal sections in A. (C) After treatment with low-Ca^{2+} medium, cells were cultured in normal Ca^{2+} medium for 30 min. The MIP of immunofluorescence confocal sections is displayed. CS, hours after Ca^{2+} switch. (D) After treatment with low-Ca^{2+} medium for 18 h, cells positive for punctate PAR3–EGFP staining were counted [at least 50 cells were counted in each sample from one experiment, with three independent experiments (n=3)]. Results are mean±s.d. (E) After 30 min of Ca^{2+} switch, ZO-1-staining was evaluated as an indicator of tight junction maturation. The percentage of cells whose surrounding ZO-1-staining was longer than half the cell perimeter was determined [at least 200 cells were counted in each sample from one experiment, with three independent experiments (n=3)]. More precise quantification is described in Fig. S5G. Clone #22 and #21 are MDCK lines expressing EGFP and nonsilencing or PAR3-knockdown shRNA, respectively. Results are mean±s.d. Student's t-test was used for statistical analysis; each blue-colored PAR3 mutant-rescued line was compared with PAR3 wild-type-rescued #4, while each red-colored PAR3 mutant-rescued line was compared with PAR3 wild-type-rescued #5. Brackets indicate other pairs analyzed by Student's t-test. 2SA indicates S852A/S889A double-mutant. Scale bars: 20 µm.

Journal of Cell Science (2020) 133, jcs244830. doi:10.1242/jcs.244830

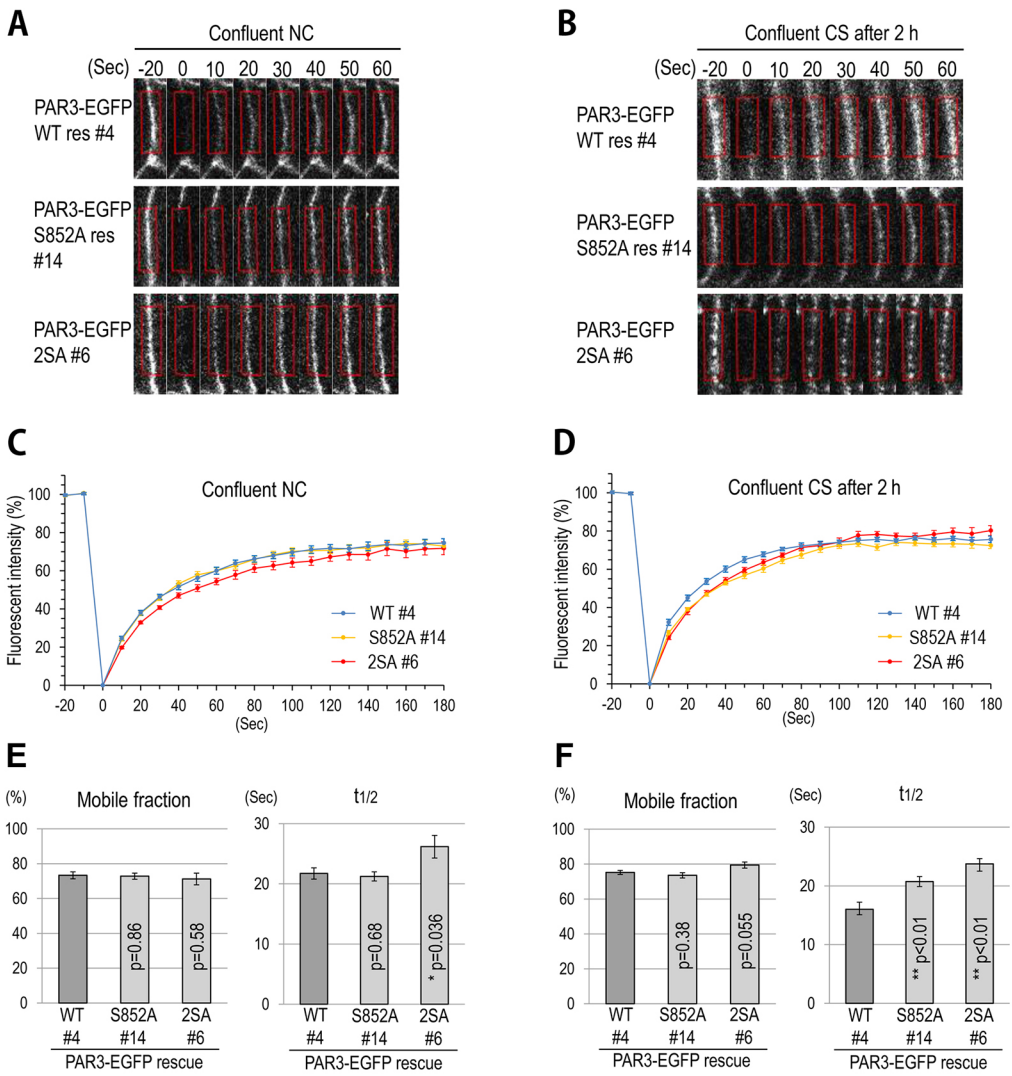

Fig. 6. FRAP analysis of PAR3 and its unphosphorylatable mutants in cell–cell junctions. (A) PAR3–EGFP-rescued cell lines were confluently cultured in normal Ca^{2+} medium (NC) and subjected to a FRAP assay. Bleaching was performed at time 0. Red rectangles represent ROIs. (B) After Ca^{2+} switch (CS), cells were cultured for 2 h. Then, they were subjected to a FRAP assay. (C) Mean±s.e.m. values of relative fluorescence intensities in experiment A were plotted (at least 10 ROIs were measured in each sample in three independent experiments). (D) Mean±s.e.m. values of relative fluorescence intensities in experiment B were plotted. (E) Mean±s.e.m. values of mobile fraction and half time of recovery in experiment A were plotted. (F) Mean±s.e.m. values of mobile fraction and half time of recovery in experiment B were plotted. Student's *t*-test was used for statistical analysis; each PAR3 mutant-rescued line was compared with PAR3 wild-type-rescued #4.

wild-type PAR3, Ser852- and/or Ser889-unphosphorylatable mutants of PAR3 tended to form clusters in the cytoplasm and to localize to the plasma membrane when the cell–cell junction was disrupted by Ca^{2+} depletion (Fig. 5A; Fig. S5E). Furthermore, these mutants not only localized to cell–cell contact sites but also mislocalized to the lateral membrane domain under normal culture conditions. Importantly, ectopic clustering and ectopic membrane localization of PAR3 appeared to be concomitant. The results of the previous report from St Johnston laboratory appear to support this notion (Benton and St Johnston, 2003b); that is, GFP-fused unphosphorylatable mutants of Bazooka/PAR3 also tend to form clusters compared with the wild-type Bazooka/PAR3 in *Drosophila* follicle cells. Taken together, these data suggest that the normal localization of PAR3 is the consequence of local clustering of PAR3 at a specific plasma membrane domain. ASPP2–PP1 complexes are probably concentrated in the PAR3 clusters, which harbor numerous ASPP2-binding sites. This, in turn, would promote ASPP2–PP1-mediated dephosphorylation of PAR3 and, consequently, clustering. Thus, this positive-feedback loop would lead to the accumulation of PAR3 at a specific membrane domain.

Phosphorylation of Ser852 or Ser889 renders PAR3 diffusive and easily accessible to the newly organized cell–cell junction. When a free PAR3 molecule reaches the cell–cell junction by diffusion, it may be efficiently dephosphorylated by an ASPP2–PP1 complex that was already associated with the localized PAR3 cluster, and oligomerize with the cluster. This mechanism may account for the observation that the turnover rates of the wild-type and unphosphorylatable mutant PAR3 were not significantly different on the mature cell–cell junction (Fig. 6E; Fig. S6B). Dephosphorylated PAR3 molecules can concentrate and exert a strong activity that promotes the formation of the tight junction and the apical domain. However, since the dephosphorylated form is less diffusive and can be trapped by some cellular structures, it fails to coordinate the rapid reconstruction of the tight junction. Therefore, both phosphorylated and dephosphorylated states are essential for the rapid recruitment and the functional integrity of PAR3 (Fig. 8).

On the basis of our observation and previous reports, dephosphorylated PAR3 can localize to several plasma membrane domains (Benton and St Johnston, 2003b; Morais-de-Sá et al., 2010). This suggests that the anchoring molecules for PAR3 are not restricted to the tight junction region. Considering this, among the several reported PAR3-binding proteins and lipids, ubiquitously distributed lipids are preferable candidates for the major membrane-anchoring factors. On this basis, Ser852 and Ser889 double-phosphorylated PAR3 could also associate with the membrane-anchoring factors, although the interaction would be unstable and transient because of the lack of clustering competency. In our hypothesis, the site where PAR3 clusters is fundamentally important for PAR3 localization. This may be defined by the

Journal of Cell Science (2020) 133, jcs244830. doi:10.1242/jcs.244830

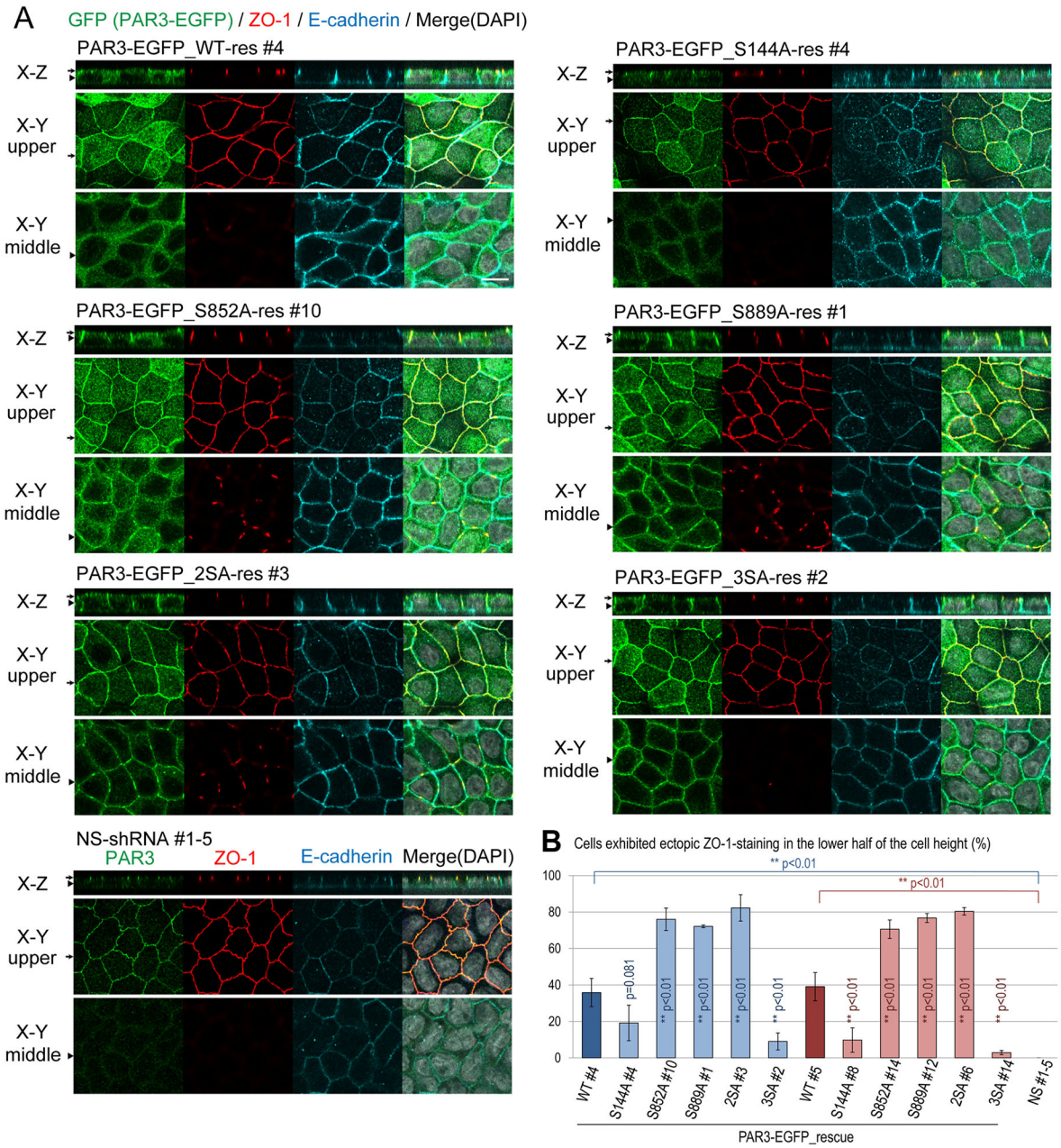

Fig. 7. Localization of PAR3 and its unphosphorylatable mutants in PAR3-rescued MDCK cell lines. (A) PAR3-rescued cell lines were cultured for 4 days (reached confluence at day 2). Immunostained samples were analyzed by confocal microscopy. Arrows on reconstituted *X*–*Z* sections indicate *Z*-positions of displayed upper *X*–*Y* planes, and arrowheads on the *X*–*Z* section indicate *Z*-positions of displayed middle *X*–*Y* planes. Arrows and arrowheads on upper and middle *X*–*Y* planes indicate where X–*Z* sections reconstituted. (B) The percentage mean±s.d. of cells exhibiting ectopic ZO-1-staining in the lower half of the cell height was determined [at least 100 cells were counted in each sample in one experiment, with three independent experiments (*n*=3)]. Student's *t*-test was used for statistical analysis; each blue-colored PAR3 mutant-rescued line was compared with PAR3 wild-type-rescued #4, while each red-colored PAR3 mutant-rescued line was compared with PAR3 wild-type-rescued #5. Brackets indicate other pairs analyzed by Student's *t*-test. 2SA and 3SA indicate S852A/S889A double-mutant and S144/S852/S889 triple-mutant, respectively. Scale bars: 10 µm.

competition between the phosphorylations by the kinases phosphorylating Ser852 and Ser889 and the dephosphorylation by the ASPP2–PP1 complex engaged to the PAR3 protein cluster. Ser852 kinases may include PAR1 (Fig. 2F–H). Other kinases, which may also localize to the basolateral membrane domain, should be identified in future studies.

Because the effects of Ser852 and Ser889 phosphorylation on clustering were similar, they appeared to be functionally redundant. However, dephosphorylation of Ser852 was primarily mediated by PP1, in contrast to Ser889, which has been reported to be primarily regulated by PP2A (Krahn et al., 2009). Thus, their upstream regulations are different, and the regulations of these sites may be context dependent. In our observations, the involvement of Ser144 phosphorylation in clustering was not significant. However, the S144A mutant failed to rescue tight junction formation after the Ca^{2+} switch, and the addition of S144A mutation abrogated the ectopic tight junction-inducing activity of PAR3-S852A/S889A (Fig. 5; Fig. 7). These results suggest that the phosphorylation of

Journal of Cell Science (2020) 133, jcs244830. doi:10.1242/jcs.244830

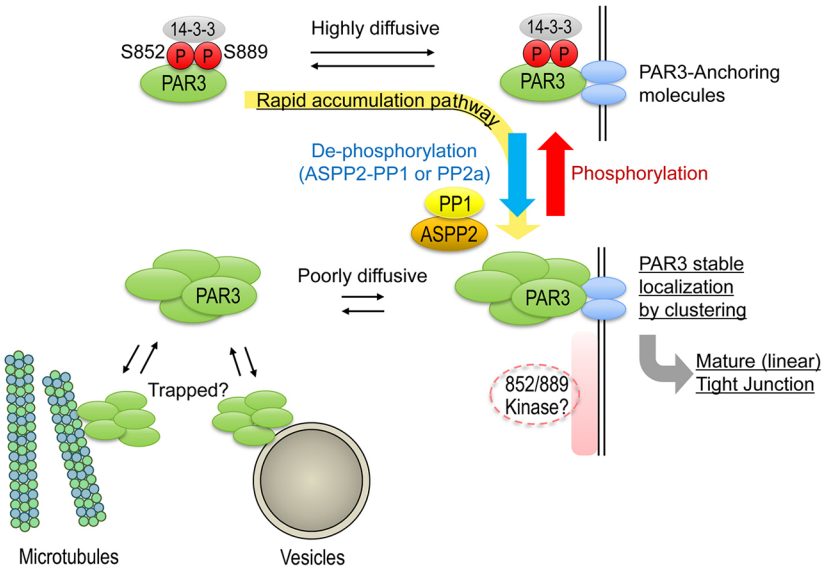

Fig. 8. Rapid and proper localization of PAR3 is achieved by the phosphorylation–dephosphorylation cycle. Phosphorylation of Ser852 and Ser889 residues permits the diffusion of PAR3 through association with 14-3-3, whereas their dephosphorylation promotes the clustering of PAR3. The increase in molecular size prevents diffusion of clustered PAR3. In addition, the association with some cellular structures may prevent diffusion of clustered PAR3. Both phosphorylation and dephosphorylation are essential for rapid recruitment and accumulation at specific sites of the membrane such as the cell–cell contact sites (yellow arrow). The balance between unidentified kinases localizing at the lateral membrane, possibly PAR1, and phosphatases, including PP1, which is associated with PAR3 through ASPP2, may determine the site where PAR3 accumulates.

Ser144 somehow positively regulates tight junction formation, although the precise mechanisms remain unknown.

The mechanism by which the phosphorylation of Ser852 and Ser889 regulates clustering remains unclear. Ser852 and Ser889 are located in the C-terminal half of PAR3, although the oligomerization domain is located at its N-terminus (Mizuno et al., 2003). The structure of the PAR3 N-terminal domain has been revealed by nuclear magnetic resonance (NMR), and the higher-order structure of oligomerized PAR3 N-terminal domain was also analyzed. The oligomers showed a filamentous structure, which is suggested to be formed by the front-to-back interaction mediated by both type I and type II PB1-like domains of the monomers (Feng et al., 2007; Zhang et al., 2013b). Although the PAR3 N-terminal domain can form filamentous oligomers by itself, the front-to-back type of interaction alone, it appears that it cannot organize massive clusters that are observed in cells. Hence, it is plausible that other molecules bind to PAR3 and bridge PAR3 oligomers (Harris, 2017), and that the phosphorylation of Ser852 and Ser889 would be involved in the regulation of this interaction.

Clustering of PAR3 has been broadly observed in several animal species. PAR3 clusters anchor centrosomes to the apical domain in the intestinal cells of *C. elegans*, the *Drosophila* embryo ectoderm without aPKC, and germline stem cells of male *Drosophila* (Feldman and Priess, 2012; Inaba et al., 2015; Jiang et al., 2015). In *C. elegans* oocytes, clustering contributes to the efficient transport of PAR3 to the anterior cortex (Rodriguez et al., 2017; Wang et al., 2017). Ser852 is likely conserved among chordates (Fig. 2E). Although the conservation of Ser852 in other species is unclear, Ser889 appears to be highly conserved among animal species (Fig. S2B). Thus, phosphorylation may be involved in the regulation of PAR3 clustering in several biological processes of various animal species. However, it has been shown that patches with accumulated Bazooka/PAR3, contain Bazooka/PAR3 molecules phosphorylated on Ser151 and/or Ser1085 in both epithelial cells and male germline stem cells of *Drosophila* (Inaba et al., 2015; Jiang et al., 2015). In addition, the data shown by Jiang et al. suggests that the Bazooka/PAR3-S151A/S1085A mutant molecules poorly accumulated into the Bazooka/PAR3 clusters. Together with our results, these observations suggest that proper expression and phosphorylation level and/or the phosphorylation–dephosphorylation cycle is important for the organization of PAR3 clusters in some contexts. Alternatively, as-yet-unidentified mechanisms may underlie cluster formation of PAR3 in those contexts. Interestingly, it has been reported that plasma membrane tension promotes the clustering of PAR3 in *C. elegans* (Wang et al., 2017). In epithelial cells, PAR3 is localized to the cell–cell junction, which is subjected to mechanical stress exerted by circumferential actin belts. On the basis of these facts, it can be speculated that dephosphorylation of PAR3 might be regulated by mechanosensing.

MATERIALS AND METHODS

Cell culture, Ca^{2+} switch and drug treatment

MDCKII cells and HEK293T cells were cultured in low-glucose Dulbecco's modified Eagle's medium supplemented with 10% fetal bovine serum and 100 U/ml penicillin/streptomycin at 37°C in a humidified atmosphere containing 5% CO_2 (Yamanaka et al., 2006, 2010). For immunofluorescence of polarized epithelial cells, 10^5 MDCK cells were cultured on permeable filters (Transwell 3460, Corning) for 4 days. Ca^{2+} switch assays were performed as previously described (Yamanaka et al., 2006). Briefly, 10^5 MDCK cells were cultured for 3 days to reach confluency. These cells were then incubated in a low-Ca^{2+} (3 µM) medium for 18 h. Then, the medium was changed to a normal growth medium (1.8 mM Ca^{2+}) to initiate junction formation. Tautomycetin was obtained from Tocris, and calyculin A was procured from Cell Signaling Technology, and were used as described in Fig. 3G.

Expression vectors, siRNAs, transfection and establishment of transformant cell lines

V5-tagged human ASPP2 full-length and fragments were amplified from V5-ASPP2-SR by PCR (Cong et al., 2010) and were subcloned into pEB6-CAG (Tanaka et al., 1999). sPAR3-SRHis, a His-T7-Xpress-tagged mouse sPAR3-expressing vector, has been described previously (Mizuno et al., 2003). sPAR3 and the long-form of rat PAR3 were subcloned into pCAG-GS-neo (Izumi et al., 1998; Yamashita et al., 2015) with an EGFP sequence to generate sPAR3–EGFP and PAR3–EGFP expression vectors, respectively. The EGFP sequence was amplified by PCR using pEGFP-N1 (Clontech) as a template. All point mutants were generated by PCR-based site-directed mutagenesis. The DNA fragment that encodes MKI-peptide (885–981 aa of *Helicobacter pylori* CagA) was artificially synthesized (Invitrogen) and subcloned into pEGFP-C1 (Clontech). pcDNA-HA-LATS2 was a kind gift from Dr Hiroshi Sasaki (Graduate School of Frontier Biosciences, Osaka University, Japan) (Ota and Sasaki, 2008). MDCK cells and HEK293T cells were transfected with plasmids

using Lipofectamine 2000 and Lipofectamine LTX (Invitrogen), respectively. ASPP2 siRNA1 #2315 and siRNA2 #3326 have been described previously (Cong et al., 2010). ASPP2 siRNA1 was used unless otherwise indicated. MDCK cells were transfected with siRNAs using Lipofectamine RNAiMAX (Invitrogen). The MDCK-transformant clones expressing nonsilencing (NS) shRNA or shRNA for ASPP2 have been described previously (Cong et al., 2010). The puromycin-resistant MDCK PAR3 knockdown clone (25a) and the nonsilencing (NS) control clone (1-5) were used in establishing PAR3–EGFP-rescued clones and EGFP-expressing control clones (#21 and #22), respectively (Yamanaka et al., 2006). To establish these clones, PAR3-EGFP-pCAG-GS-neo and its point mutants were transfected to PAR3-knockdown cells and selected in 800 µg/ml G418-containing medium.

Antibodies

The rabbit anti-ASPP2 antibodies C2AP and C3AP have been described previously (Cong et al., 2010). Anti-phospho-PAR3 Ser827 has also been described previously (Nagai-Tamai et al., 2002). The antibodies specific for PAR3 phosphorylated on Ser852 and Ser889 were raised by immunization of rabbits with the keyhole limpet hemocyanin-conjugated phosphopeptides KSKpSMDLGIC and KSSpSLESLQC, respectively, and were affinity-purified. Anti-GST has been described previously (Izumi et al., 1998). Anti-PAR3 (07-330, Upstate), anti-T7 (69522, Novagen), and anti-PP2Ac (05-421, Upstate) were purchased from Merck Millipore. Omni probe, anti-His-T7-Xpress-tag (sc-7270 and sc-499), anti-PP1α (sc-7482), anti-pan 14-3-3 (sc-629), anti-aPKC (sc-216), anti-PAR6β (sc-67392), anti-ZO-1 (sc-33725), and normal rabbit IgG (sc-2027) were purchased from Santa Cruz Biotechnology. Anti-V5 (R960-25), anti-claudin1 (71-7800), and anti-occludin (71-1500) were procured from Invitrogen. Anti-phospho-aPKCζ Thr410 (9378), anti-myosin light chain 2 (3672), anti-phospho-myosin light chain 2 (3674), anti-phospho-Ser 14-3-3-binding motif (9606), and anti-phospho-threonine (9386) were obtained from Cell Signaling Technology. Anti-aPKC (610176) and anti-E-cadherin (610181) were purchased from BD BioScience. Anti-GAPDH (ab8245) was obtained from abcam, anti-YAP1 (H00010413-M01) was purchased from Abnova, anti-GFP (598) was procured from MBL, and anti-HA (3F10) was obtained from Roche. See also Table S1 for information about usages and conditions.

Immunofluorescence and quantification of fluorescent signals

Cells were fixed with 2% paraformaldehyde in PBS and permeabilized with 0.5% Triton X-100 in PBS. After incubation with a primary antibody, cells were stained with Alexa Fluor-conjugated secondary antibodies (Invitrogen). F-actin was stained with Rhodamine–phalloidin. Images were obtained using an epifluorescence microscope (AxioImager, Carl Zeiss) or a confocal laser scanning microscope system (LSM700, Carl Zeiss). ImageJ software was used for the quantification of fluorescent signals. Regions of interest (ROIs) were defined as described in Fig. S1B and Fig. S4.

Immunoprecipitation and far-western blotting

HEK293T or MDCK cells were lysed in a buffer containing 25 mM Tris-HCl (pH 7.5), 140 mM NaCl, 2.5 mM $MgCl_2$, 1 mM ethylene glycol tetraacetic acid, 0.5% Triton X-100, Complete protease inhibitor cocktail (Roche), and PhosSTOP phosphatase inhibitor cocktail (Roche). After centrifugation (20,000 ***g*** for 10 min) the supernatants were subjected to immunoprecipitation with the indicated antibodies, followed by SDS-PAGE and western blotting. His-T7-Xpress-tagged PAR3 mutants were immunoprecipitated by using anti-T7 antibody, separated by SDS-PAGE, and then transferred to a PVDF membrane. For probing with 14-3-3 proteins, the membrane was soaked in a denature buffer (50 mM Tris-HCl, pH 8.3, 7 M guanidine, 50 mM dithiothreitol, 2 mM EDTA) for 1 h and then renatured in a renature buffer (20 mM Tris-HCl, pH 7.4, 140 mM NaCl, 4 mM dithiothreitol, 1 mM $MgCl_2$, 10 µM $ZnCl_2$, 0.1% bovine serum albumin, 0.1% Nonidet P-40) at 4°C for 4 h. After blocking with 4% skim milk in the renature buffer for 4 h, the membrane was incubated with 10 µg/ml of GST–14-3-3ζ in the renature buffer at 4°C overnight and then subjected to immunoblotting using an anti-GST antibody.

FRAP analysis

Time-lapse imaging was performed using a confocal microscopy system (Axio imager and LSM700, Carl Zeiss) equipped with a 40× dipping objective (Carl Zeiss) and a culture chamber (INUG2-UK, Tokai Hit).

Cells were maintained at 37°C in FluoroBrite DMEM (Gibco) supplemented with 10% FBS under 5% CO_2 conditions. ROIs were set on cell–cell contacts, where PAR3–EGFP is concentrated. Fluorescence of EGFP was bleached with a 100% power laser and measured with a 0.5% power laser. Images were obtained every 10 s. The fluorescence intensity immediately after bleaching was considered as the background level, and the half time of recovery ($t_{1/2}$) was calculated by curve-fitting to the equation $I(t)=I_{max}\bullet(1-e^{-kt})$, where $k=\ln 2/t_{1/2}$, using the Solver tool of Excel (Microsoft).

In vitro kinase assay and *in vitro* dephosphorylation assay

The kinase assay was performed as previously described (Yamashita et al., 2010). His-T7-Xpress-tagged PAR1b was overexpressed in COS1 cells and immunoprecipitated with anti-T7 antibody and then used as the kinase source in this experiment. For the *in vitro* dephosphorylation assay, the substrate PAR3 was immunoprecipitated from confluent cultured MDCK cells using anti-PAR3 antibody. Bead-immobilized substrate was washed with PMP buffer (50 mM HEPES, pH 7.5, 100 mM NaCl, 2 mM DTT, 0.01% Brij 35, 1 mM $MnCl_2$), and PP1α (New England Biolab) was added and incubated for 30 min at 30°C. Then, the phosphorylation levels of PAR3 were analyzed by western blotting.

Statistical analysis

Differences were considered statistically significant when $P<0.05$ as assessed using a two-tailed unpaired Student's *t*-test. Student's *t*-tests were performed using Excel (Microsoft). Single asterisk and double asterisks denote $P<0.05$ and $P<0.01$, respectively. The results are presented as mean±s.d., unless otherwise indicated.

Acknowledgements

We thank Dr H. Sasaki (Osaka University) for providing the materials and the members of Ohno laboratory for their helpful comments.

Competing interests

The authors declare no competing or financial interests.

Author contributions

Conceptualization: K.Y., K.M., S.O.; Validation: K.Y.; Formal analysis: K.Y.; Investigation: K.Y., K.M., K.F., H.H., N.S., M.M.-H., Y.A., A.S.; Resources: T.H., A.S.; Writing - original draft: K.Y.; Writing - review & editing: K.M., T.H., S.O.; Supervision: T.H.; Project administration: S.O.; Funding acquisition: K.Y., K.M., S.O.

Funding

This work was supported in part by the grant for Creation of Innovation Centers for Advanced Interdisciplinary Research Areas Program from the Ministry of Education, Culture, Sports, Science and Technology of Japan (to S.O.), Japan Society for the Promotion of Science (JSPS) KAKENHI (JP23112003 to S.O., JP13670129 to K.M. and JP17K17991 to K.Y.), and the Yokohama Foundation for Advancement of Medical Science (to K.Y.).

Supplementary information

Supplementary information available online at
https://jcs.biologists.org/lookup/doi/10.1242/jcs.244830.supplemental

Peer review history

The peer review history is available online at
https://jcs.biologists.org/lookup/doi/10.1242/jcs.244830.reviewer-comments.pdf

References

Benton, R. and St Johnston, D. (2003a). A conserved oligomerization domain in drosophila Bazooka/PAR-3 is important for apical localization and epithelial polarity. *Curr. Biol.* **13**, 1330-1334. doi:10.1016/S0960-9822(03)00508-6

Benton, R. and St Johnston, D. (2003b). Drosophila PAR-1 and 14-3-3 inhibit Bazooka/PAR-3 to establish complementary cortical domains in polarized cells. *Cell* **115**, 691-704. doi:10.1016/S0092-8674(03)00938-3

Betschinger, J., Mechtler, K. and Knoblich, J. A. (2003). The Par complex directs asymmetric cell division by phosphorylating the cytoskeletal protein Lgl. *Nature* **422**, 326-330. doi:10.1038/nature01486

Bilder, D., Schober, M. and Perrimon, N. (2003). Integrated activity of PDZ protein complexes regulates epithelial polarity. *Nat. Cell Biol.* **5**, 53-58. doi:10.1038/ncb897

Chen, X. and Macara, I. G. (2005). Par-3 controls tight junction assembly through the Rac exchange factor Tiam1. *Nat. Cell Biol.* **7**, 262-269. doi:10.1038/ncb1226

Chen, X. and Macara, I. G. (2006). Par-3 mediates the inhibition of LIM kinase 2 to regulate cofilin phosphorylation and tight junction assembly. *J. Cell Biol.* **172**, 671-678. doi:10.1083/jcb.200510061

Chen, S., Chen, J., Shi, H., Wei, M., Castaneda-Castellanos, D. R., Bultje, R. S., Pei, X., Kriegstein, A. R., Zhang, M. and Shi, S.-H. (2013). Regulation of microtubule stability and organization by mammalian Par3 in specifying neuronal polarity. *Dev. Cell* **24**, 26-40. doi:10.1016/j.devcel.2012.11.014

Choy, M. S., Swingle, M., D'Arcy, B., Abney, K., Rusin, S. F., Kettenbach, A. N., Page, R., Honkanen, R. E. and Peti, W. (2017). PP1:Tautomycetin complex reveals a path toward the development of PP1-specific inhibitors. *J. Am. Chem. Soc.* **139**, 17703-17706. doi:10.1021/jacs.7b09368

Cong, W., Hirose, T., Harita, Y., Yamashita, A., Mizuno, K., Hirano, H. and Ohno, S. (2010). ASPP2 regulates epithelial cell polarity through the PAR complex. *Curr. Biol.* **20**, 1408-1414. doi:10.1016/j.cub.2010.06.024

Drewes, G., Ebneth, A., Preuss, U., Mandelkow, E.-M. and Mandelkow, E. (1997). MARK, a novel family of protein kinases that phosphorylate microtubule-associated proteins and trigger microtubule disruption. *Cell* **89**, 297-308. doi:10.1016/S0092-8674(00)80208-1

Ebnet, K., Suzuki, A., Horikoshi, Y., Hirose, T., Meyer Zu Brickwedde, M. K., Ohno, S. and Vestweber, D. (2001). The cell polarity protein ASIP/PAR-3 directly associates with junctional adhesion molecule (JAM). *EMBO J.* **20**, 3738-3748. doi:10.1093/emboj/20.14.3738

Egloff, M.-P., Johnson, D. F., Moorhead, G., Cohen, P. T., Cohen, P. and Barford, D. (1997). Structural basis for the recognition of regulatory subunits by the catalytic subunit of protein phosphatase 1. *EMBO J.* **16**, 1876-1887. doi:10.1093/emboj/16.8.1876

Etemad-Moghadam, B., Guo, S. and Kemphues, K. J. (1995). Asymmetrically distributed PAR-3 protein contributes to cell polarity and spindle alignment in early C. elegans embryos. *Cell* **83**, 743-752. doi:10.1016/0092-8674(95)90187-6

Feldman, J. L. and Priess, J. R. (2012). A role for the centrosome and PAR-3 in the hand-off of MTOC function during epithelial polarization. *Curr. Biol.* **22**, 575-582. doi:10.1016/j.cub.2012.02.044

Feng, W., Wu, H., Chan, L.-N. and Zhang, M. (2007). The Par-3 NTD adopts a PB1-like structure required for Par-3 oligomerization and membrane localization. *EMBO J.* **26**, 2786-2796. doi:10.1038/sj.emboj.7601702

Fletcher, G. C., Lucas, E. P., Brain, R., Tournier, A. and Thompson, B. J. (2012). Positive feedback and mutual antagonism combine to polarize Crumbs in the Drosophila follicle cell epithelium. *Curr. Biol.* **22**, 1116-1122. doi:10.1016/j.cub.2012.04.020

Harris, T. J. C. (2017). Protein clustering for cell polarity: Par-3 as a paradigm. *F1000Res* **6**, 1620. doi:10.12688/f1000research.11976.1

Harris, T. J. and Peifer, M. (2004). Adherens junction-dependent and -independent steps in the establishment of epithelial cell polarity in Drosophila. *J. Cell Biol.* **167**, 135-147. doi:10.1083/jcb.200406024

Harris, T. J. C. and Peifer, M. (2005). The positioning and segregation of apical cues during epithelial polarity establishment in Drosophila. *J. Cell Biol.* **170**, 813-823. doi:10.1083/jcb.200505127

Helps, N. R., Barker, H. M., Elledge, S. J. and Cohen, P. T. (1995). Protein phosphatase 1 interacts with p53BP2, a protein which binds to the tumour suppressor p53. *FEBS Lett.* **377**, 295-300. doi:10.1016/0014-5793(95)01347-4

Hirose, T., Izumi, Y., Nagashima, Y., Tamai-Nagai, Y., Kurihara, H., Sakai, T., Suzuki, Y., Yamanaka, T., Suzuki, A., Mizuno, K. et al. (2002). Involvement of ASIP/PAR-3 in the promotion of epithelial tight junction formation. *J. Cell Sci.* **115**, 2485-2495.

Höfling, F. and Franosch, T. (2013). Anomalous transport in the crowded world of biological cells. *Rep. Prog. Phys.* **76**, 046602. doi:10.1088/0034-4885/76/4/046602

Horikoshi, Y., Suzuki, A., Yamanaka, T., Sasaki, K., Mizuno, K., Sawada, H., Yonemura, S. and Ohno, S. (2009). Interaction between PAR-3 and the aPKC-PAR-6 complex is indispensable for apical domain development of epithelial cells. *J. Cell Sci.* **122**, 1595-1606. doi:10.1242/jcs.043174

Horikoshi, Y., Hamada, S., Ohno, S. and Suetsugu, S. (2011). Phosphoinositide binding by par-3 involved in par-3 localization. *Cell Struct. Funct.* **36**, 97-102. doi:10.1247/csf.11005

Hurd, T. W., Fan, S., Liu, C.-J., Kweon, H. K., Hakansson, K. and Margolis, B. (2003). Phosphorylation-dependent binding of 14-3-3 to the polarity protein Par3 regulates cell polarity in mammalian epithelia. *Curr. Biol.* **13**, 2082-2090. doi:10.1016/j.cub.2003.11.020

Inaba, M., Venkei, Z. G. and Yamashita, Y. M. (2015). The polarity protein Baz forms a platform for the centrosome orientation during asymmetric stem cell division in the Drosophila male germline. *Elife* **4**, e04960. doi:10.7554/eLife.04960.011

Izumi, Y., Hirose, T., Tamai, Y., Hirai, S., Nagashima, Y., Fujimoto, T., Tabuse, Y., Kemphues, K. J. and Ohno, S. (1998). An atypical PKC directly associates and colocalizes at the epithelial tight junction with ASIP, a mammalian homologue of Caenorhabditis elegans polarity protein PAR-3. *J. Cell Biol.* **143**, 95-106. doi:10.1083/jcb.143.1.95

Jiang, T., McKinley, R. F., McGill, M. A., Angers, S. and Harris, T. J. (2015). A Par-1-Par-3-centrosome cell polarity pathway and its tuning for isotropic cell adhesion. *Curr. Biol.* **25**, 2701-2708. doi:10.1016/j.cub.2015.08.063

Jouette, J., Guichet, A. and Claret, S. B. (2019). Dynein-mediated transport and membrane trafficking control PAR3 polarised distribution. *Elife* **8**, e40212. doi:10.7554/eLife.40212

Kemphues, K. J., Priess, J. R., Morton, D. G. and Cheng, N. S. (1988). Identification of genes required for cytoplasmic localization in early C. elegans embryos. *Cell* **52**, 311-320. doi:10.1016/S0092-8674(88)80024-2

Knoblich, J. A. (2001). Asymmetric cell division during animal development. *Nat. Rev. Mol. Cell Biol.* **2**, 11-20. doi:10.1038/35048085

Krahn, M. P., Egger-Adam, D. and Wodarz, A. (2009). PP2A antagonizes phosphorylation of Bazooka by PAR-1 to control apical-basal polarity in dividing embryonic neuroblasts. *Dev. Cell* **16**, 901-908. doi:10.1016/j.devcel.2009.04.011

Krahn, M. P., Klopfenstein, D. R., Fischer, N. and Wodarz, A. (2010). Membrane targeting of Bazooka/PAR-3 is mediated by direct binding to phosphoinositide lipids. *Curr. Biol.* **20**, 636-642. doi:10.1016/j.cub.2010.01.065

Lippincott-Schwartz, J., Snapp, E. and Kenworthy, A. (2001). Studying protein dynamics in living cells. *Nat. Rev. Mol. Cell Biol.* **2**, 444-456. doi:10.1038/35073068

Liu, C.-Y., Lv, X., Li, T., Xu, Y., Zhou, X., Zhao, S., Xiong, Y., Lei, Q.-Y. and Guan, K.-L. (2011). PP1 cooperates with ASPP2 to dephosphorylate and activate TAZ. *J. Biol. Chem.* **286**, 5558-5566. doi:10.1074/jbc.M110.194019

Mitsuhashi, S., Matsuura, N., Ubukata, M., Oikawa, H., Shima, H. and Kikuchi, K. (2001). Tautomycetin is a novel and specific inhibitor of serine/threonine protein phosphatase type 1, PP1. *Biochem. Biophys. Res. Commun.* **287**, 328-331. doi:10.1006/bbrc.2001.5596

Mizuno, K., Suzuki, A., Hirose, T., Kitamura, K., Kutsuzawa, K., Futaki, M., Amano, Y. and Ohno, S. (2003). Self-association of PAR-3-mediated by the conserved N-terminal domain contributes to the development of epithelial tight junctions. *J. Biol. Chem.* **278**, 31240-31250. doi:10.1074/jbc.M303593200

Morais-de-Sá, E., Mirouse, V. and St Johnston, D. (2010). aPKC phosphorylation of Bazooka defines the apical/lateral border in Drosophila epithelial cells. *Cell* **141**, 509-523. doi:10.1016/j.cell.2010.02.040

Nagai-Tamai, Y., Mizuno, K., Hirose, T., Suzuki, A. and Ohno, S. (2002). Regulated protein-protein interaction between aPKC and PAR-3 plays an essential role in the polarization of epithelial cells. *Genes Cells* **7**, 1161-1171. doi:10.1046/j.1365-2443.2002.00590.x

Nešić, D., Miller, M. C., Quinkert, Z. T., Stein, M., Chait, B. T. and Stebbins, C. E. (2010). Helicobacter pylori CagA inhibits PAR1-MARK family kinases by mimicking host substrates. *Nat. Struct. Mol. Biol.* **17**, 130-132. doi:10.1038/nsmb.1705

Ohno, S. (2001). Intercellular junctions and cellular polarity: the PAR-aPKC complex, a conserved core cassette playing fundamental roles in cell polarity. *Curr. Opin. Cell Biol.* **13**, 641-648. doi:10.1016/S0955-0674(00)00264-7

Ota, M. and Sasaki, H. (2008). Mammalian Tead proteins regulate cell proliferation and contact inhibition as transcriptional mediators of Hippo signaling. *Development* **135**, 4059-4069. doi:10.1242/dev.027151

Rodriguez, J., Peglion, F., Martin, J., Hubatsch, L., Reich, J., Hirani, N., Gubieda, A. G., Roffey, J., Fernandes, A. R., St Johnston, D. et al. (2017). aPKC Cycles between functionally distinct PAR protein assemblies to drive cell polarity. *Dev. Cell* **42**, 400-415.e9. doi:10.1016/j.devcel.2017.07.007

Román-Fernández, A. and Bryant, D. M. (2016). Complex polarity: building multicellular tissues through apical membrane traffic. *Traffic* **17**, 1244-1261. doi:10.1111/tra.12417

Rotem, S., Katz, C. and Friedler, A. (2007). Insights into the structure and protein-protein interactions of the pro-apoptotic protein ASPP2. *Biochem. Soc. Trans.* **35**, 966-969. doi:10.1042/BST0350966

Saadat, I., Higashi, H., Obuse, C., Umeda, M., Murata-Kamiya, N., Saito, Y., Lu, H., Ohnishi, N., Azuma, T., Suzuki, A. et al. (2007). Helicobacter pylori CagA targets PAR1/MARK kinase to disrupt epithelial cell polarity. *Nature* **447**, 330-333. doi:10.1038/nature05765

Salomon, J., Gaston, C., Magescas, J., Duvauchelle, B., Canioni, D., Sengmanivong, L., Mayeux, A., Michaux, G., Campeotto, F., Lemale, J. et al. (2017). Contractile forces at tricellular contacts modulate epithelial organization and monolayer integrity. *Nat. Commun.* **8**, 13998. doi:10.1038/ncomms13998

Suzuki, A. and Ohno, S. (2006). The PAR-aPKC system: lessons in polarity. *J. Cell Sci.* **119**, 979-987. doi:10.1242/jcs.02898

Suzuki, A., Ishiyama, C., Hashiba, K., Shimizu, M., Ebnet, K. and Ohno, S. (2002). aPKC kinase activity is required for the asymmetric differentiation of the premature junctional complex during epithelial cell polarization. *J. Cell Sci.* **115**, 3565-3573. doi:10.1242/jcs.00032

Suzuki, A., Hirata, M., Kamimura, K., Maniwa, R., Yamanaka, T., Mizuno, K., Kishikawa, M., Hirose, H., Amano, Y., Izumi, N. et al. (2004). aPKC acts upstream of PAR-1b in both the establishment and maintenance of mammalian epithelial polarity. *Curr. Biol.* **14**, 1425-1435. doi:10.1016/j.cub.2004.08.021

Tabuse, Y., Izumi, Y., Piano, F., Kemphues, K. J., Miwa, J. and Ohno, S. (1998). Atypical protein kinase C cooperates with PAR-3 to establish embryonic polarity in Caenorhabditis elegans. *Development* **125**, 3607-3614.

Tanaka, J., Miwa, Y., Miyoshi, K., Ueno, A. and Inoue, H. (1999). Construction of Epstein-Barr virus-based expression vector containing mini-oriP. *Biochem. Biophys. Res. Commun.* **264**, 938-943. doi:10.1006/bbrc.1999.1617

Tanentzapf, G. and Tepass, U. (2003). Interactions between the crumbs, lethal giant larvae and bazooka pathways in epithelial polarization. *Nat. Cell Biol.* **5**, 46-52. doi:10.1038/ncb896

Tepass, U., Tanentzapf, G., Ward, R. and Fehon, R. (2001). Epithelial cell polarity and cell junctions in Drosophila. *Annu. Rev. Genet.* **35**, 747-784. doi:10.1146/annurev.genet.35.102401.091415

Traweger, A., Wiggin, G., Taylor, L., Tate, S. A., Metalnikov, P. and Pawson, T. (2008). Protein phosphatase 1 regulates the phosphorylation state of the polarity scaffold Par-3. *Proc. Natl. Acad. Sci. USA* **105**, 10402-10407. doi:10.1073/pnas.0804102105

Vigneron, A. M., Ludwig, R. L. and Vousden, K. H. (2010). Cytoplasmic ASPP1 inhibits apoptosis through the control of YAP. *Genes Dev.* **24**, 2430-2439. doi:10.1101/gad.1954310

Wang, S.-C., Low, T. Y. F., Nishimura, Y., Gole, L., Yu, W. and Motegi, F. (2017). Cortical forces and CDC-42 control clustering of PAR proteins for Caenorhabditis elegans embryonic polarization. *Nat. Cell Biol.* **19**, 988-995. doi:10.1038/ncb3577

Yamanaka, T., Horikoshi, Y., Sugiyama, Y., Ishiyama, C., Suzuki, A., Hirose, T., Iwamatsu, A., Shinohara, A. and Ohno, S. (2003). Mammalian Lgl forms a protein complex with PAR-6 and aPKC independently of PAR-3 to regulate epithelial cell polarity. *Curr. Biol.* **13**, 734-743. doi:10.1016/S0960-9822(03)00244-6

Yamanaka, T., Horikoshi, Y., Izumi, N., Suzuki, A., Mizuno, K. and Ohno, S. (2006). Lgl mediates apical domain disassembly by suppressing the PAR-3-aPKC-PAR-6 complex to orient apical membrane polarity. *J. Cell Sci.* **119**, 2107-2118. doi:10.1242/jcs.02938

Yamashita, K., Suzuki, A., Satoh, Y., Ide, M., Amano, Y., Masuda-Hirata, M., Hayashi, Y. K., Hamada, K., Ogata, K. and Ohno, S. (2010). The 8th and 9th tandem spectrin-like repeats of utrophin cooperatively form a functional unit to interact with polarity-regulating kinase PAR-1b. *Biochem. Biophys. Res. Commun.* **391**, 812-817. doi:10.1016/j.bbrc.2009.11.144

Yamashita, K., Ide, M., Furukawa, K. T., Suzuki, A., Hirano, H. and Ohno, S. (2015). Tumor suppressor protein Lgl mediates G1 cell cycle arrest at high cell density by forming an Lgl-VprBP-DDB1 complex. *Mol. Biol. Cell* **26**, 2426-2438. doi:10.1091/mbc.E14-10-1462

Yu, C. G. and Harris, T. J. C. (2012). Interactions between the PDZ domains of Bazooka (Par-3) and phosphatidic acid: in vitro characterization and role in epithelial development. *Mol. Biol. Cell* **23**, 3743-3753. doi:10.1091/mbc.e12-03-0196

Zhang, M., Yogesha, S. D., Mayfield, J. E., Gill, G. N. and Zhang, Y. (2013a). Viewing serine/threonine protein phosphatases through the eyes of drug designers. *FEBS J.* **280**, 4739-4760. doi:10.1111/febs.12481

Zhang, Y., Wang, W., Chen, J., Zhang, K., Gao, F., Gao, B., Zhang, S., Dong, M., Besenbacher, F., Gong, W. et al. (2013b). Structural insights into the intrinsic self-assembly of Par-3 N-terminal domain. *Structure* **21**, 997-1006. doi:10.1016/j.str.2013.04.004

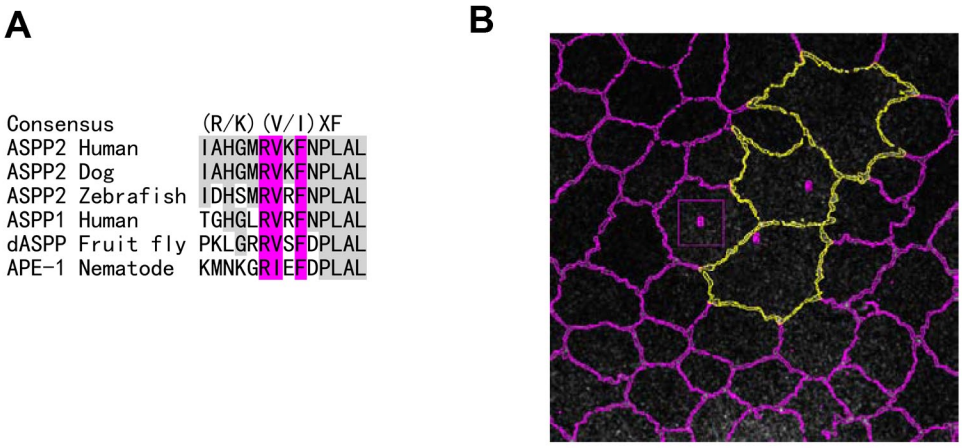

Figure S1. Yamashita K et al.

Fig. S1. Related to Fig. 1. (A) Sequence alignment of the PP1-binding consensus sequence in ASPP2 and its homologs. Magenta indicates the consensus PP1-binding sequence. (B) Optical sections were obtained at 0.4-µm intervals by confocal microscopy. Among sections, ZO-1-positive sequential four slices were projected. A tight junction region was defined by thresholding and binarizing ZO-1-staining (magenta). By manual deletion of a V5-negative region, ROI was generated (yellow). Relative intensity was calculated by dividing [mean of magenta] by [mean of yellow]. A background signal was subtracted for quantification.

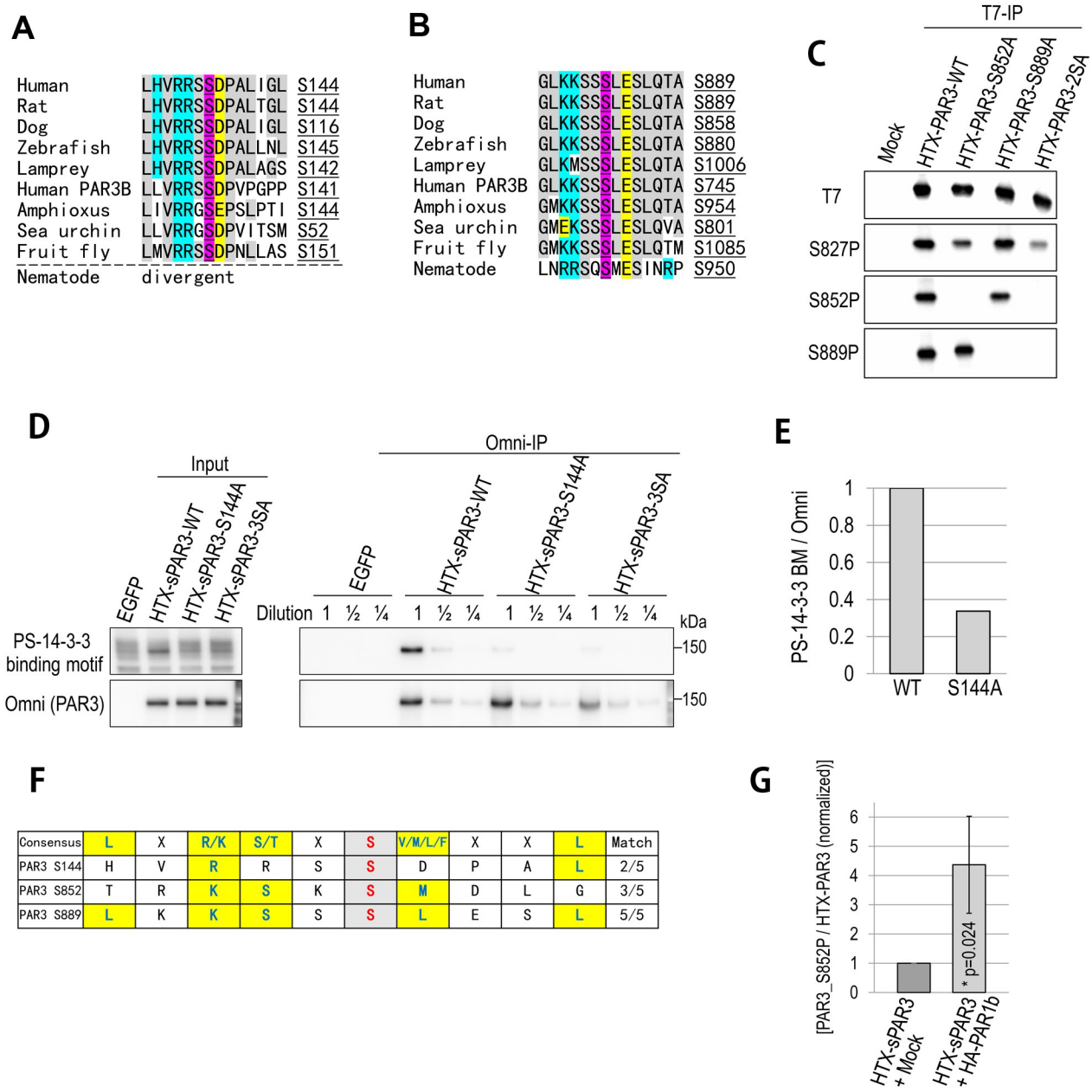

Figure S2. Yamashita K et al.

Fig. S2. Related to Fig. 2. (A) Sequence alignment around Ser144 of PAR3. (B) Sequence alignment around Ser889 of PAR3. (C) PAR3 and its point mutants were exogenously expressed in MDCK cells and immunoprecipitated. Specificity of phosphorylated serine-specific antibodies was confirmed by western blotting. (D) His-T7-Xpress-tagged wild-type PAR3, PAR3-S144A, and PAR3-3SA (S144A/S852A/S889A) were exogenously expressed in MDCK cells and immunoprecipitated. Then, western blotting was performed. The 14-3-3-binding motif antibody primarily recognized the phosphorylation of Ser144 in PAR3. (E) Quantification of the signal using 14-3-3-binding motif antibody. Signal intensity was normalized by total HTX-PAR3 (Omni). (F) The consensus sequence of the PAR1 substrate and the sequence around S144, S852, and S889 of PAR3. (G) PAR1b overexpression-mediated phosphorylation of Ser852 of PAR3 was quantified.

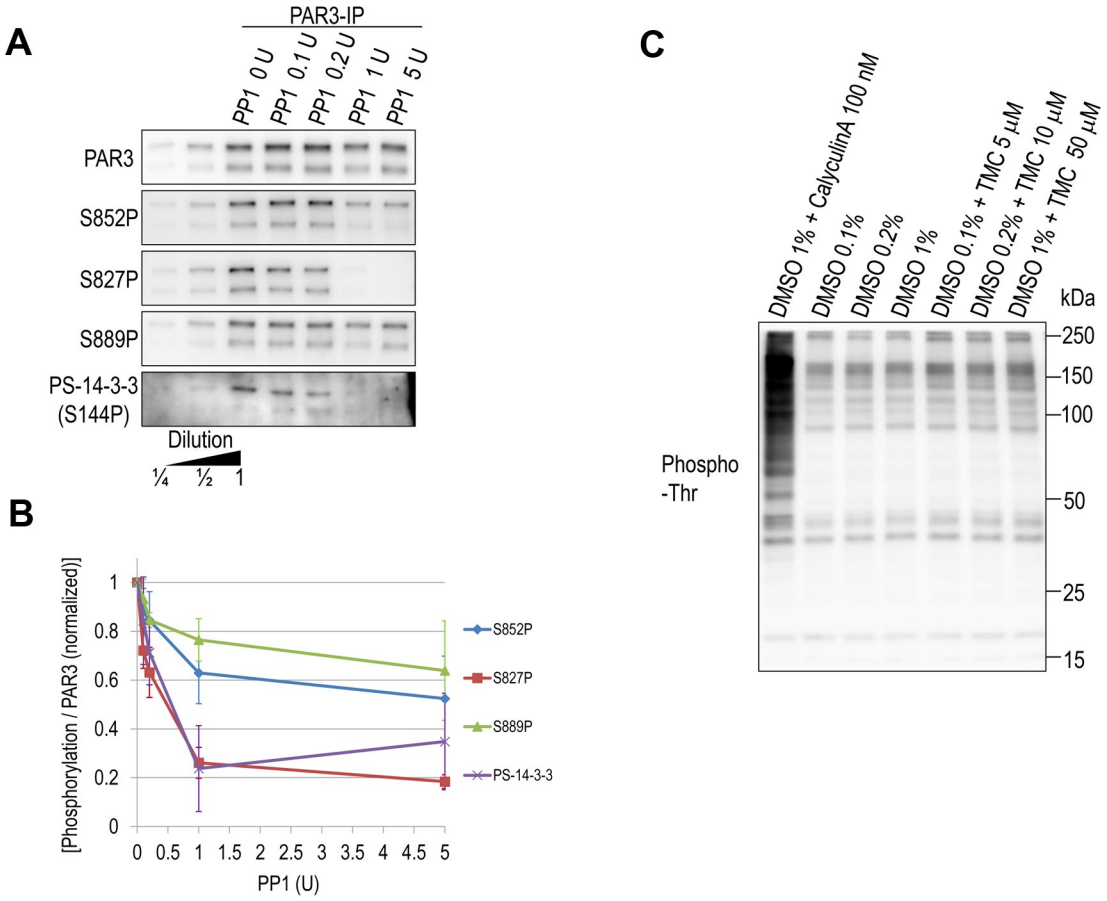

Figure S3. Yamashita K et al.

Fig. S3. Related to Fig. 3. (A) PAR3 was immunopurified from MDCK cells, and recombinant PP1α was treated. After incubation, the phosphorylation levels were assayed by western blotting. (B) Quantification of PAR3 phosphorylation in experiment A (n = 3). (C) MDCK cells were treated with the broad phosphatase inhibitor calyculin A and the PP1-specific inhibitor tautomycetin (TMC) for 1 h using DMSO as a vehicle. Calyculin A broadly promoted a variety of protein phosphorylation, whereas the effect of tautomycetin appeared to be confined.

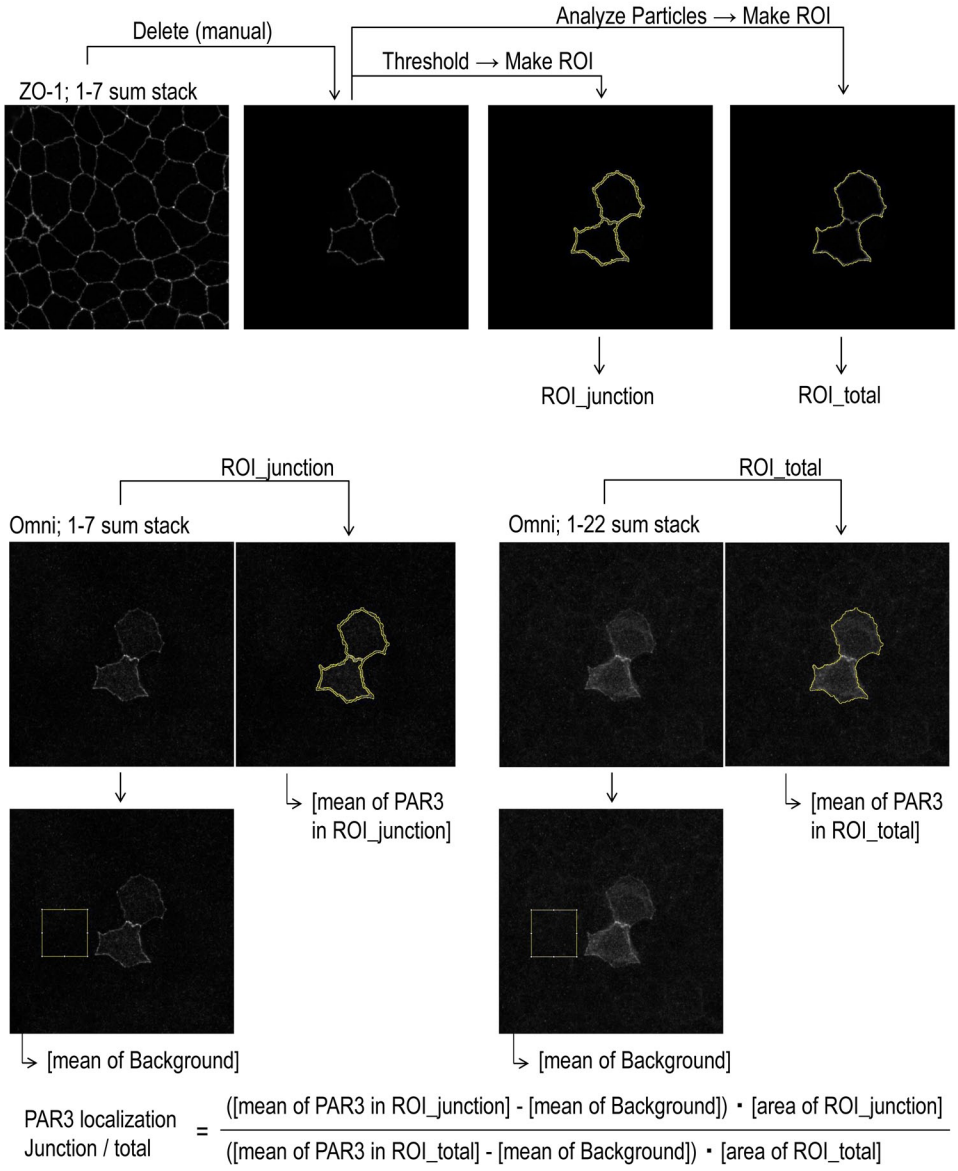

Figure S4. Yamashita K et al.

Fig. S4. Related to Fig. 4. Optical sections were obtained at 0.4-μm intervals by confocal microscopy. Among sections, ZO-1-positive sequential sections were projected. A tight junction region was defined by thresholding and binarizing ZO-1-staining. After deleting Omni-negative cells, ROI was generated (ROI_junction). On the other hand, ROI_total was generated by applying analyze particle tool to z-projection of ZO-1-staining. For quantification, the background signal was subtracted.

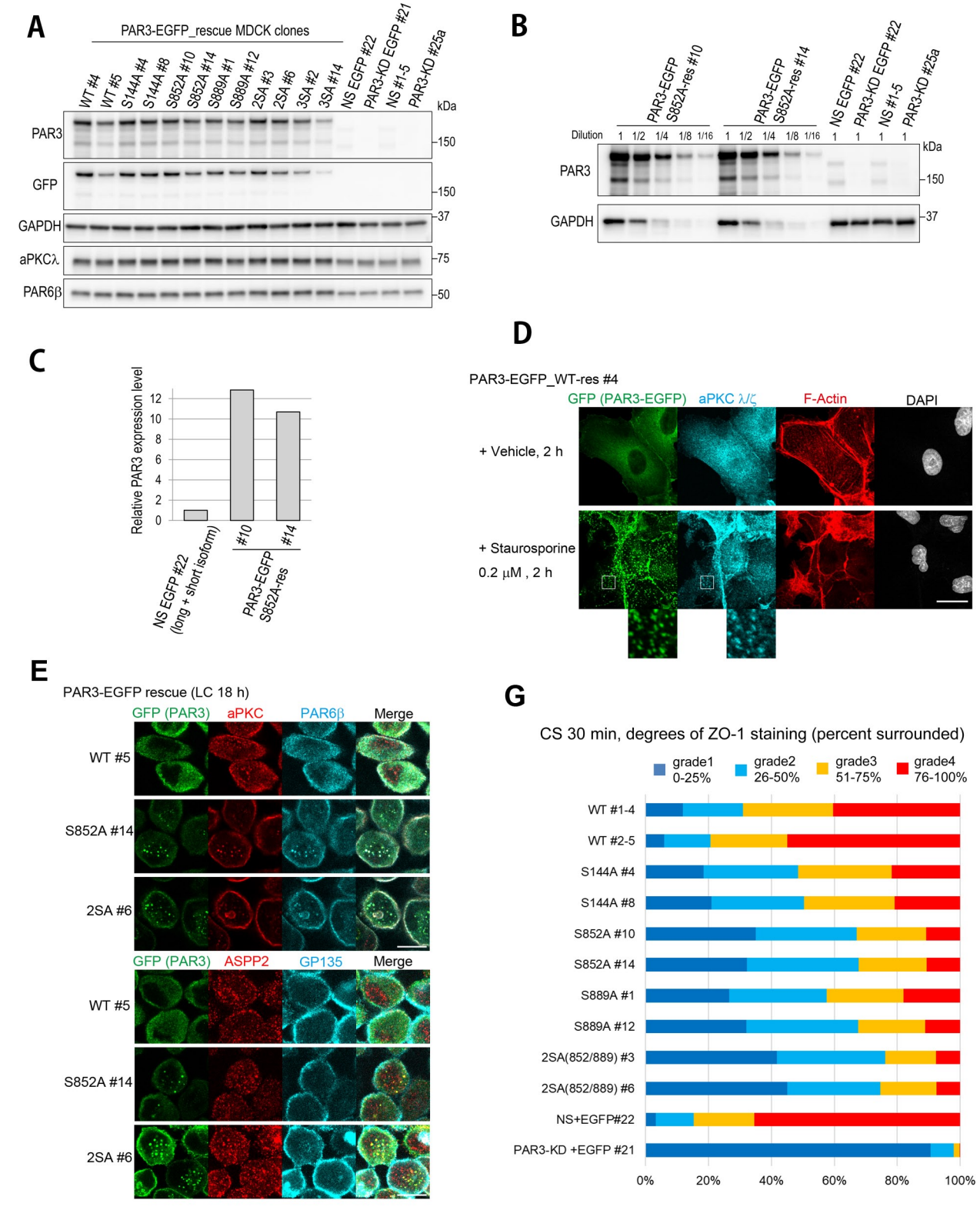

Figure S5. Yamashita K et al.

Fig. S5. Related to Fig. 5. (A) Expression levels of PAR3-EGFP in PAR3-rescued cells. Whole cell lysates of indicated cell lines were analyzed. 10 μg/lane of proteins was used. 2SA and 3SA indicate S852A/S889A double-mutant and S144A/S852A/S889A triple-mutant, respectively. (B) Whole cell lysates of PAR3-EGFP-S852A-rescued cells were diluted and compared to the endogenous level. (C) Densitometric analysis of the result in (B). Signals from endogenously expressed long and short PAR3 isoforms were integrated. (D) PAR3-WT-EGFP-rescued cells were treated with 0.2 μM staurosporine for 2 h. Punctate staining of PAR3-EGFP and aPKC was evident by staurosporine treatment. (E) PAR3-rescued MDCK cell lines were cultured in low-calcium medium for 18 h. Then, immunofluorescence staining was performed. One confocal section is displayed. (F) After 2 h of calcium switch, immunofluorescence staining was performed. The MIP of immunofluorescent confocal sections is displayed. (G) After 30 min of calcium switch, ZO-1-staining was evaluated as an indicator of tight junction maturation. Degrees of surrounding ZO-1-staining are indicated by colors. Cell populations are represented with length of bars (average of three independent experiments). Scale bars represent 20 μm.

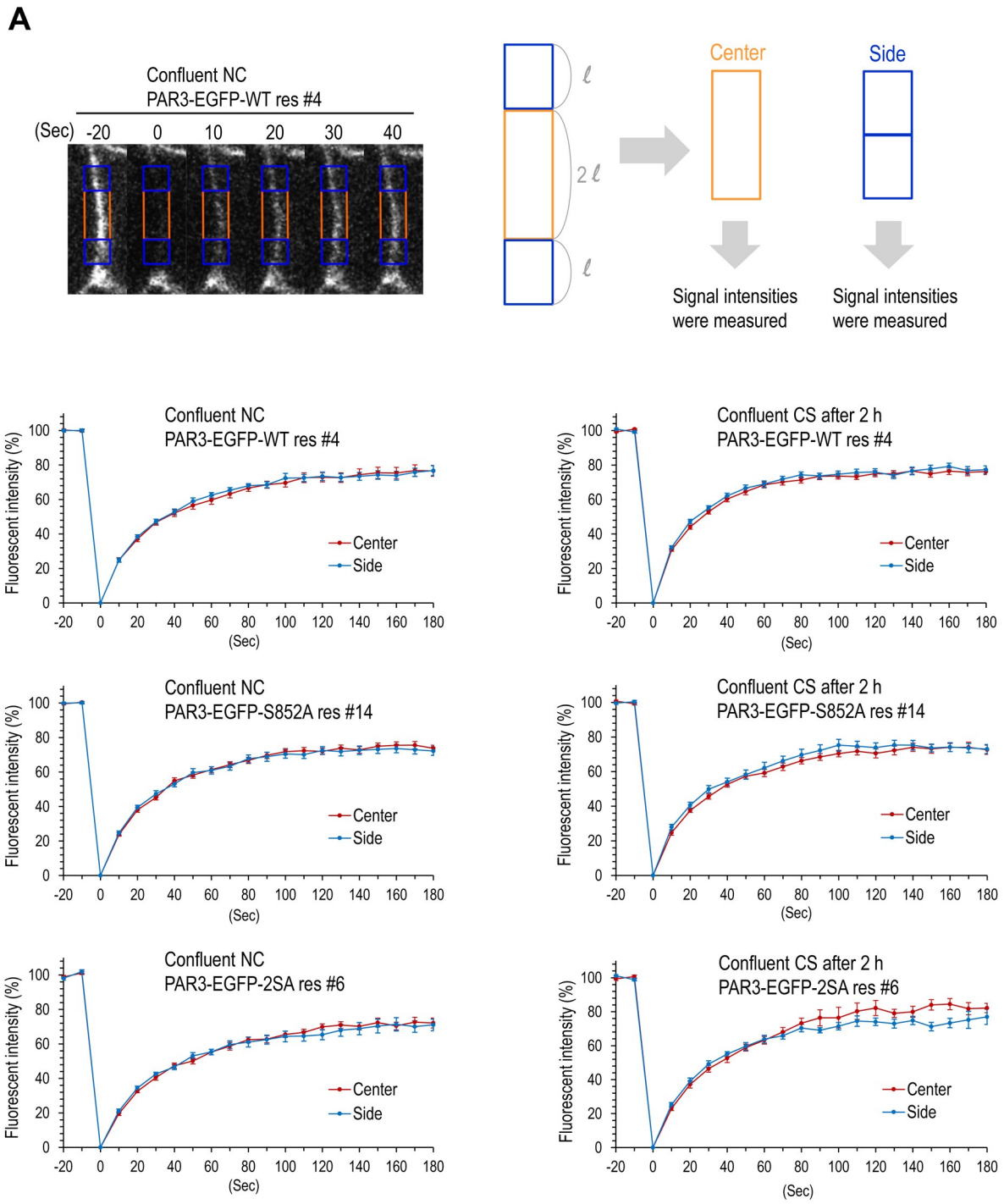

Figure S6. Yamashita K et al.

Fig. S6. Related to Fig. 6. (A) The fluorescent recovery adjacent to unbleached membrane region (side) and that in distal region (center) were compared. Uniform recovery was observed in each PAR3-rescued line and both culture conditions. (B, C) PAR3-EGFP-rescued cell lines were confluently cultured in normal calcium medium and subjected to FRAP assay. Average values of mobile fraction and half time of recovery were plotted. Residual transformant clones were used, which were not used in Fig. 6. Student's t-test was used for statistical analysis; each PAR3 mutant-rescued line was compared with PAR3 wild-type-rescued #5. Error bars represent ± standard error (SE).

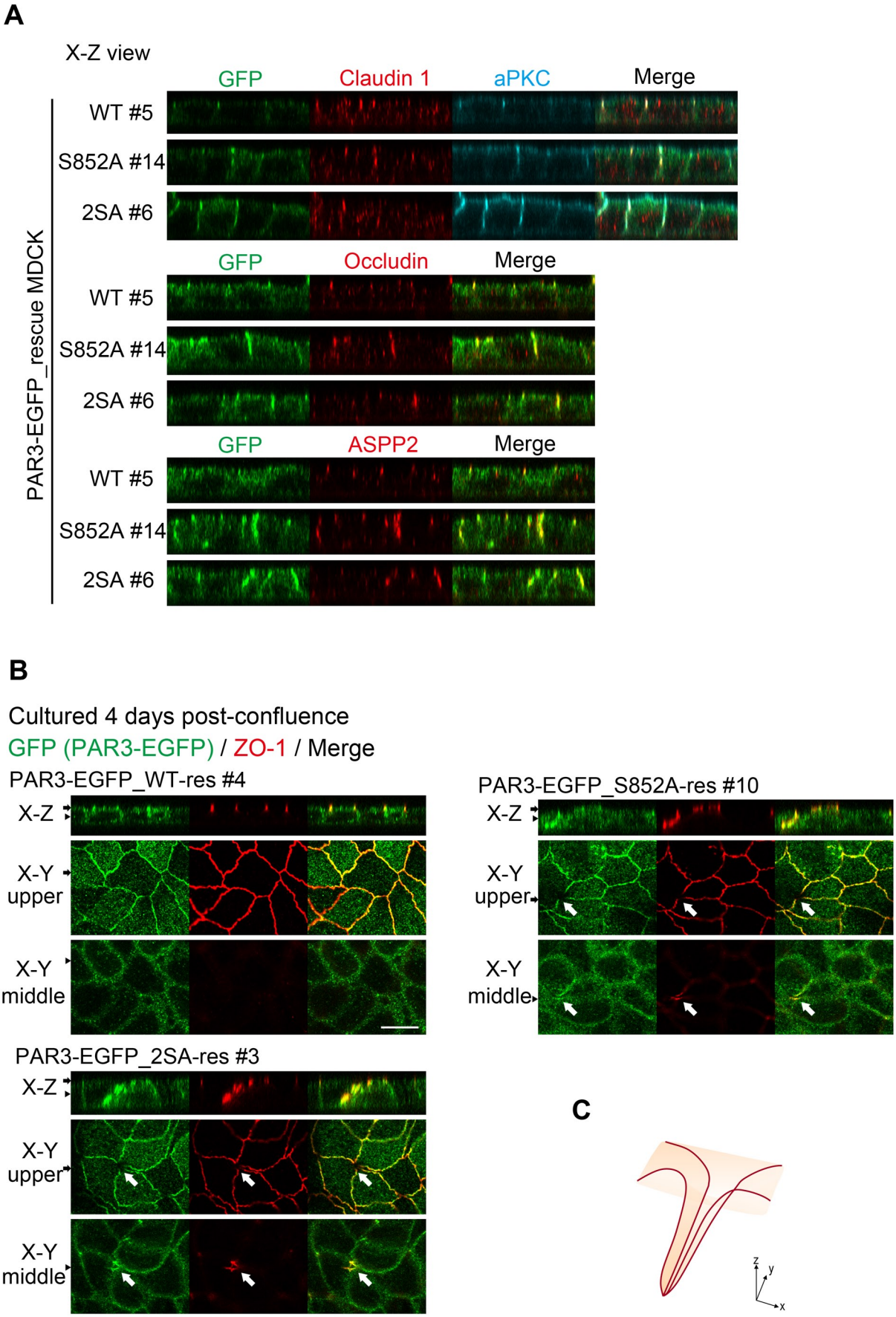

Figure S7. Yamashita K et al.

Fig. S7. Related to Fig. 7. (A) PAR3-rescued cell lines were cultured for 4 days (reached confluence at day 2). Immunostained samples were analyzed by confocal microscopy, and reconstituted X–Z sections are shown. Tight junction components were partially colocalized with unphosphorylatable PAR3 mutants at the lateral membrane domains. (B) PAR3-rescued cell lines were cultured for 6 days (reached confluence at day 2). Immunostained samples were analyzed by confocal microscopy. Black arrows and arrowheads are placed in the same manner as in Fig. 7A. White arrows indicate tubular invaginations. (C) Expected 3D structure of the tubular invaginations. Lines represent tight junctions.

Table S1. List of antibodies used in this study.

Antibodies	Host	Source	Cat#	Application/Dillution
anti-PAR3	Rabbit	Upstate (Merck)	07-330	WB (1:500), IF (1:300), IP (2μg)
anti-phospho-PAR3 Ser827	Rabbit	Nagai-Tamai et al., 2002	N/A	WB (1:300)
anti-phospho-PAR3 Ser852	Rabbit	This study	N/A	WB (1:100)
anti-phospho-PAR3 Ser889	Rabbit	This study	N/A	WB (1:500)
anti-ASPP2	Rabbit	Cong et al., 2010	N/A	WB (1:1000), IF (1:1000)
anti-PP1α	Mouse	Santa Cruz Biotechnology	sc-7482	WB (1:200)
anti-PP2A C subunit	Mouse	Upstate (Merck)	05-421	WB (1:1000)
anti-aPKC	Rabbit	Santa Cruz Biotechnology	sc-216	WB (1:1000), IF (1:300)
anti-aPKC	Mouse	BD BioSciences	610176	WB (1:1000)
anti-phospho-aPKCζ Thr410	Rabbit	Cell Signaling Technology	9378	WB (1:500)
anti-PAR6β	Rabbit	Santa Cruz Biotechnology	sc-67392	WB (1:1000), IF (1:500)
anti-pan 14-3-3	Rabbit	Santa Cruz Biotechnology	sc-629	WB (1:1000)
anti-ZO-1	Rat	Santa Cruz Biotechnology	sc-33725	IF (1:300)
anti-claudin1	Rabbit	Zymed (Thermo Fisher Scientific)	71-7800	IF (1:200)
anti-occludin	Rabbit	Zymed (Thermo Fisher Scientific)	71-1500	IF (1:200)
anti-E-cadherin	Mouse	BD BioSciences	610181	IF (1:500)
anti-myosin light chain 2	Rabbit	Cell Signaling Technology	3672	WB (1:500)
anti-phospho-myosin light chain 2	Rabbit	Cell Signaling Technology	3674	WB (1:500)
anti-phospho-Ser 14-3-3-binding motif	Mouse	Cell Signaling Technology	9606	WB (1:100)
anti-phospho-threonine	Mouse	Cell Signaling Technology	9386	WB (1:1000)
anti-V5	Mouse	Invitrogen (Thermo Fisher Scientific)	R960-25	WB (1:1000), IF (1:500), IP (2μg)
Omni probe (anti-His-T7-Xpress-tag)	Mouse	Santa Cruz Biotechnology	sc-7270	WB (1:1000), IF (1:300)
Omni probe (anti-His-T7-Xpress-tag)	Rabbit	Santa Cruz Biotechnology	sc-499	WB (1:1000), IP (2μg)
anti-T7	Mouse	Novagen (Merck)	69522	WB (1:5000), IP (2μg)
anti-GFP	Rabbit	MBL	598	WB (1:1000)
anti-GFP	Chick	aves Labs	GFP-1010	IF (1:5000)
anti-HA (3F10)	Rat	Roche (Merck)	11867423001	WB (1:500)
anti-GST	Rabbit	Izumi et al., 1998	N/A	WB (1:1000)
anti-GAPDH	Mouse	abcam	ab8245	WB (1:200000)
anti-YAP1	Mouse	Abnova	H00010413-M01	WB (1:1000)
Normal rabbit IgG	Rabbit	Santa Cruz Biotechnology	sc-2027	IP (2μg)